Methods[1]

Expedition 340 Scientists[2]

Chapter contents

Introduction

Information in this chapter will help the reader understand the basis for shipboard observations and preliminary conclusions for Integrated Ocean Drilling Program (IODP) Expedition 340. It will also enable the interested investigator to identify data and select samples for further analysis. Information presented here concerns only shipboard operations and analyses described in the site chapters (Sites U1393–U1401). This introductory section provides an overview of shipboard operations, curatorial conventions, and general core handling and analysis. Methods used by various investigators for shore-based analyses of Expedition 340 samples and data will be described in individual publications in various professional journals and the **"Expedition research results"** chapters of this *Proceedings* volume.

Site locations

At all Expedition 340 sites, GPS coordinates from precruise site surveys were used to position the R/V *JOIDES Resolution.* The only seismic system used during the cruise was the Syquest Bathy 2010 CHIRP subbottom profiler, which was monitored on the approach to each site to ascertain that the seafloor depth agreed with that from the precruise survey. Once the vessel was positioned at a site, the thrusters were lowered and a positioning beacon was dropped to the seafloor. The dynamic positioning control of the vessel uses navigational input from the GPS and triangulation to the seafloor beacon, weighted by the estimated positional accuracy. The final hole position was calculated from the mean position of the GPS data collected over the time that the hole was occupied.

Coring and drilling operations

The advanced piston corer (APC) and extended core barrel (XCB) were used during Expedition 340. These standard coring systems and their characteristics are summarized in Graber et al. (2002). The APC cuts soft sediment cores with minimal coring disturbance relative to other IODP coring systems. After the APC core barrel is lowered through the drill pipe and lands near the bit, the drill pipe is pressurized until the two shear pins that hold the inner barrel attached to the outer barrel fail. The inner barrel then advances with minimal rotation into the formation and cuts the core. The driller can detect a successful cut, or "full stroke," from the pressure gauge on the rig floor. The XCB is deployed when the

formation becomes too stiff or too hard for the APC. The XCB cutting shoe (bit) extends as far as ~30.5 cm ahead of the main bit in soft sediments but retracts into the main bit if hard formations are encountered. The XCB is a rotary system with a small cutting shoe extending below the large rotary drill bit. The smaller bit can cut a semiindurated core with less torque and fluid circulation than the main bit and thus optimizes recovery.

In situ temperature measurements were made by replacing the standard APC cutting shoe with the advanced piston corer temperature tool (APCT-3). The APCT-3 includes a battery pack, a data logger, and a temperature sensor. During deployment, the APC inner core barrel is lowered to the mudline, where it typically sits for 5 min before being lowered to the bottom of the borehole and penetrating the sediment. The core barrel is then decoupled from the drill string and left stationary to record temperature. Heat is generated by friction produced during penetration. Temperature is therefore measured every 2 s continuously for 5–10 min after firing so that the decay of the thermal disturbance is recorded, allowing the formation temperature to be calculated. During this time, fluid circulation within the hole is turned off so that temperature measurements are not affected. The APCT-3 could therefore only be used when hole conditions were stable. Finally, the coring shoe and barrel are extracted and returned to the deck where data is recovered from the data logger. Formation temperature measurements were made using the APCT-3 at Sites U1395–U1400 (see "Downhole logging").

APC refusal is conventionally defined in two ways: (1) the piston fails to achieve a complete stroke (as determined from the pump pressure reading) because the formation is too hard or (2) excessive force (>60,000 lb; ~267 kN) is required to pull the core barrel out of the formation. When a full or partial stroke is achieved but excessive force cannot retrieve the barrel, the core barrel can be "drilled over": after the inner core barrel is successfully shot into the formation, the drill bit is advanced to total depth to free the APC barrel. This strategy allows a hole to be advanced much further with the APC, the preferred coring tool. Nonmagnetic core barrels are commonly used during APC coring to reduce magnetic overprinting of paleomagnetic measurements; these cores can be orientated using the FlexIt tool (see "Paleomagnetism"). Standard steel core barrels are used when utilizing the drillover technique because they are stronger than nonmagnetic barrels. The XCB is used to advance the hole when APC refusal occurs before the target depth is reached. Most APC/XCB cored intervals are ~9.5 m long, which is the length of a standard core barrel. However, the amount of advance during coring varies. Core operations and recovery information are given in the "Operations" section of each site chapter.

The bottom-hole assembly (BHA) is the lowermost part of the drill string. The exact configuration of the BHA is reported in the "Operations" section of each site chapter. A typical APC/XCB BHA consists of a drill bit (11⁷⁄₁₆ inch outer diameter), a bit sub, a seal bore drill collar, a landing saver sub, a modified top sub, a modified head sub, a nonmagnetic drill collar (for APC/XCB), a number of 8 inch (~20.32 cm) drill collars, a tapered drill collar, six joints (two stands) of 5½ inch (~13.97 cm) drill pipe, and one crossover sub.

Downhole logging operations were conducted in Holes U1394, U1395, U1397, and U1399 (see "Downhole logging").

Curatorial procedures and sample depth calculations

Numbering of sites, holes, cores, and samples followed standard IODP procedure (Fig. F1). Drilling sites are numbered consecutively from the first site drilled by the *Glomar Challenger* in 1968. IODP Expedition 301 began using the prefix "U" to designate sites occupied by the US Implementing Organization (USIO) vessel, the *JOIDES Resolution*. For all IODP drill sites, a letter suffix distinguishes each hole cored at the same site. The first hole cored is assigned the site number modified by the suffix "A," the second hole takes the site number and the suffix "B," and so forth. For Expedition 340, each site has two or more cored holes (A, B, C, etc.).

A full curatorial identifier for a sample consists of the following information: expedition, site, hole, core number, core type, section number, and interval in centimeters measured from the top of the core section and also the sampling tools and volumes taken. For example, in sediment, a sample identification of "340-U1394B-1H-2, 10–12 cm" represents a sample taken from the interval between 10 and 12 cm below the top of Section 2 of Core 1 ("H" designates that this core was taken with the APC system) of Hole B of Site U1394 during Expedition 340. For cores taken with the XCB, the core type is indicated by an "X" after the core number. Drilled intervals are assigned double-digit numbers, and the cores recovered after a drilled interval are assigned the following number in combination with the corresponding letter for drilling/coring system. For example, the drilled interval in Hole U1396B was designated 340-U1396B-11, where the first "1" indicates drilled interval 1 and the second "1" indicates the first section of that interval that was drilled. The first core recovered in Hole U1396B after the drilled interval was designated 340-U1396B-2H ("H" for APC).

The cored interval is measured in meters below seafloor (mbsf) according to the core depth below seafloor, method A (CSF-A), depth scale (see IODP Depth Scale Terminology at **www.iodp.org/program-policies/**). In general, the depth below seafloor is determined by subtracting the water depth estimated from the initial drill pipe measurement to the seafloor from the total drill pipe measurement. The depth interval assigned to an individual core begins with the depth below seafloor at which coring began and extends to the depth that coring advanced. Each coring interval is generally ~9.5 m, which is the length of a core barrel; however, coring intervals may be shorter or longer because of sediment expansion. Method B (CSF-B) corrects for sediment expansion, mathematically ensuring depth overlap does not occur between sections.

During Expedition 340, unless otherwise noted, all core depths below seafloor have been calculated as CSF-A and all depths have been calculated as CSF-B for plotting physical properties. For ease of communication of shipboard results, all depths are reported in this volume as "mbsf" unless otherwise noted.

Core handling and analysis

As soon as cores arrived on deck, they were extracted from the core barrel in plastic liners. These liners were carried from the rig floor to the core processing area on the catwalk outside the Core Laboratory, where they were split into ~1.5 m sections. Core catchers were sampled for biostratigraphic analyses. Liner caps (blue = top; colorless = bottom) were placed onto cut liner sections on the catwalk by the curator. Hard rock pieces were pushed to the top of the liner sections and total rock length was measured. The length was entered into the database using the SampleMaster application as "created" length. Created length is used to calculate recovery. Headspace samples were taken from the freshly exposed end of a core section using a brass boring tool for immediate hydrocarbon analysis as part of the shipboard safety and pollution prevention program (see **"Geochemistry"**).

Cores were processed on the catwalk, and whole-round sections were routinely taken and transferred immediately to the Geochemistry Laboratory for a wide range of geochemical and microbiological subsampling, including interstitial water extraction (see **"Geochemistry"**). Once subsampling was completed, the remaining pieces of whole-round core sections were brought back to the Core Laboratory for routine core processing.

As described in **"Lithostratigraphy," "Physical properties,"** and **"Paleomagnetism,"** routine core processing in the Core Laboratory included whole-round logging of core sections and core splitting.

Twenty-four whole-round samples from all sites were taken for geotechnical analyses following whole-round logging but before core splitting.

Core sections were split lengthwise in the core splitting room to expose the split core surface. The length of each section of core, including spacers, was entered into the curation database as curated length. Curated length commonly differs by a few to several centimeters from the created length measured on the catwalk. The database recalculates the assumed depth of each piece based on the curated length. The working half is defined by the double lines scribed on the outside of the core liner and denoted by a "W" after the core section in the full identifier (e.g., 340-U1396B-2H-5W); "A" is used to denote the archive half.

Archive-half sections were then imaged with the Section Half Image Logger (SHIL), measured for point source magnetic susceptibility and reflectance using the Section Half Multisensor Logger (SHMSL), measured for natural remanent magnetization (NRM) both before and after alternating field (AF) demagnetization with the superconducting rock magnetometer (SRM), and visually described for lithologic and petrological properties. The working halves were sampled for standard shipboard analyses including smear slides, moisture and density (MAD) samples, paleomagnetic cubes, nannofossils, percent carbonate, total carbon, and X-ray diffraction (XRD) analyses. The working half split section was measured for shear strength and *P*-wave velocity. Taking of personal research samples was deferred to an expedition sampling party at the IODP Gulf Coast Repository in College Station, Texas (USA) in August 2012.

After completing routine core processing, both halves of the core were wrapped in plastic wrap, put into labeled plastic tubes, sealed, and transferred to cold storage space aboard the ship. At the end of the expedition, the cores and samples were transferred from the ship to refrigerated containers and shipped to cold storage at the Gulf Coast Repository.

Drilling-induced core deformation

Cores may be significantly disturbed and contain extraneous material as a result of the coring and core handling process. Therefore, the top 10–50 cm of each core must be carefully examined for potential "fall-in" during description. Common coring-induced deformation includes concave-downward appearance of originally horizontal bedding. In APC cores, the motion of the piston may result in fluidization (flow-in) at the bottom of the cores. Retrieval from depth to the surface may result in elastic rebound. Observed core disturbances are described in the "Lithostratigraphy" section in each site chapter and

graphically indicated on the core summary graphic reports (barrel sheets; see "Core descriptions").

Lithostratigraphy

This section outlines the procedures used to document the composition, texture, alteration, and sedimentary structure of geologic materials recovered during Expedition 340. These procedures include visual core description, graphical core logging, smear slide and petrographic thin section description, digital color imaging, and color spectrophotometry. Because many of the geologic techniques and observations used to analyze sedimentary material are similar to those used to analyze igneous material, the methods for both are presented together. All acquired data were uploaded into the IODP-USIO Laboratory Information Management System (LIMS), and observations were entered using the DESClogik application in Tabular Data Capture mode. For consistency, our procedures and database templates closely followed the methods for core descriptions from recent IODP volcanic and volcaniclastic expeditions, in particular IODP Expedition 330, Louisville Seamount Trail (Expedition 330 Scientists, 2012), and IODP Expedition 334, Costa Rica Seismogenesis Project (Expedition 334 Scientists, 2012).

Core sections available for sedimentary, petrographic, and structural observation and interpretation included both working and archive halves. Sections dominated by soft sediment were split using a thin wire held in high tension. Pieces of hard rock were split with a diamond-impregnated saw so that important compositional and structural features were preserved in both the archive and working halves. The split surface of the archive half was then assessed for quality (e.g., smearing or surface unevenness) and, if necessary, scraped lightly with a glass slide or spatula. After splitting, the archive half was imaged with the SHIL and then analyzed for color reflectance and magnetic susceptibility using the SHMSL.

Following imaging, the first step in describing the recovered core was identifying unit boundaries on the basis of lithologic changes, color, grain size, the presence of volcaniclastic sediment or sedimentary intercalations, structure, and alteration. Archive sections of sediment cores were macroscopically described for lithologic, sedimentary, volcanic, and structural features. Lithostratigraphic units were characterized by visual inspection; smear slide samples were used to determine sedimentary constituents and abundances to aid in lithologic classification.

Based on preliminary visual descriptions and physical properties data, thin section samples and samples for XRD and inductively coupled plasma–atomic emission spectroscopy (ICP-AES) were extracted from working half sections. All descriptions and sample locations were recorded using curated depths and then documented on visual core description (VCD) graphic reports. A graphical core log of the core was also hand drawn, scanned, and added to the VCD (see "Graphical core logs").

DESClogik application

Descriptive data were input into the LIMS database using the DESClogik tabular entry application.

The DESClogik Expedition 340 Core Description template consists of a spreadsheet with a series of tabs. Key features expected to occur in the cores were grouped together in a General tab. These features represented observations that were made for every interval cored. More detailed information could be added into other tabs as needed for specific intervals.

The General tab included all information necessary to generate a VCD: drilling disturbance intensity, major lithology (and abundance and maximum grain size), minor lithology (and abundance and maximum grain size), clast percentage, percentage of seven clast types (see "Clast textural types"), clast angularity, matrix alteration intensity, deformation structures, and structural strike and dip.

The remaining template tabs were used to record clast composition; macroscopic structures; tephra layers; veins, vesicles, and halos; smear slides; alteration; thin section mineralogy, alteration, and structure; and so on. A brief synthesis of the section was recorded in the Section summary tab, and a summary of the entire core was recorded in the Core summary tab.

Drilling disturbance

Drilling disturbance indicates the intensity of sediment disturbance caused by the drilling process. The degree of disturbance within soft sediment is characterized using the nomenclature of Ocean Drilling Program (ODP) Leg 180 (Taylor, Huchon, Klaus, et al., 2000):

- Slightly disturbed: bedding contacts are slightly deformed.
- Moderately disturbed: bedding contacts have undergone extreme bowing.
- Extremely disturbed: bedding is completely deformed as flow-in and other soft stretching and/or compressional shearing structures attributed to coring/drilling.

Major and minor lithologies

Major and minor lithologies were chosen from standard ODP/IODP lithology terminology (Fig. F2). In

some cases the lithology (e.g., basaltic) needed to be divided by texture (e.g., pumiceous). The DESClogik value list initially contained every lithology ever encountered during IODP drilling, but this extensive list was simplified to those lithologies that were likely to be encountered during this expedition. This simplification was helpful when we described large numbers of core sections in short periods of time.

Clast percentage

Clast percentage refers to the percentage area covered by clasts within the described interval.

Clast textural types

Seven types of clasts were identified in the core: pumice, scoria, lava-massive, lava-vesicular, volcaniclastic (reworked), sedimentary, and other (Fig. F3).

1. Pumice clasts have white to yellow color. These clasts are generally poorly angular to rounded, as they result from pumice fallout and pumice pyroclastic flows. They are highly vesiculated (≤80%). Vesicles are generally spherical to subspherical. Glass is poorly microcrystallized.

2. Scoria clasts have a dark color and an irregular shape and are vesiculated to poorly vesiculated with large and irregular vesicles. The largest vesicles result from the coalescence of smaller ones. The groundmass is always microcrystalline.

3. Massive lava clasts are dense and without vesicles. They are gray to dark in color depending on composition (andesite to basaltic andesite) (LeBas et al., 1992) and alteration. In some cases when they are oxidized they take on a red color. They are generally phenocryst rich (35%–55%). They are part of massive lava domes and, in only a few cases, of lava flows.

4. Vesiculated lava clasts have the same characteristics as massive lava clasts but contain more or less abundant vesicles. They result mainly from the outer parts of lava domes or from superficial parts of lava flows. They can have a scoriaceous aspect.

5. Volcaniclastic clasts are sedimentary facies composed of volcanic (mainly pyroclastic) material. This material may include ash, lapilli, blocks, bombs, and tuffs.

6. Sedimentary clasts are composed of limestone. Limestones are white carbonate rocks from the coral platform.

7. The category "other clasts" contains all the clasts not described before: cumulates originating from magma chambers, hydrothermalized lavas from hydrothermal systems, basic enclaves, and mud clasts. In Expedition 340 cores, mud clasts and hydrothermalized lavas from hydrothermal systems are the dominant clasts observed in this category.

Grain size

Grain size refers to the coarse tail (maximum size) of the matrix. Sizes of outsized clasts are described in a separate data entry. The following grain sizes were used in DESClogik for the matrix:

- Very fine mud,
- Fine mud (where silt grains were not visible),
- Silt-fine-mud (grains visible but human eye cannot quantify size),
- Very fine sand (<187 µm),
- Fine sand (<250 µm),
- Fine medium sand (<375 µm),
- Medium sand (<500 µm),
- Coarse sand (<1 mm),
- Very coarse sand (1–2 mm),
- Granules (2–4 mm), and
- Pebbles (4–64 mm).

Sedimentary structures

Sedimentary structures include those formed by the migration of bedforms or by action of organisms (bioturbation) and may include features such as ripple cross-lamination or planar lamination. When possible, the strike and dip of such features were noted. Figure F3 contains the full set of sedimentary structures seen within the cores.

Alteration intensity

Alteration characteristics were described from visual observations of the core section archive halves (Fig. F3). The core description team adopted a basic methodology that involved identifying what was altered (e.g., debris avalanche block, avalanche matrix, or lava clasts) the degree of alteration, and alteration color. Color identification was achieved using simplified names based on Munsell Soil Color Charts (Munsell Color Company, Inc., 1994). Notes on the form of alteration (e.g., veins or halos) and the alteration mineral assemblages were recorded. However, detailed descriptions and identifications were not deemed necessary for achieving Expedition 340 scientific objectives and were therefore not completed on board the ship. These descriptions can be determined on shore at a later date if necessary.

Degree of alteration is represented graphically on the VCDs as alteration intensity and is defined according to the following ranges:

Fresh = <2 vol%.
Slight–moderate = 2–10 vol%.
Moderate–high = >10–50 vol%.
High–complete = >50–100 vol%.

Graphical core logs

Describing sequences of clastic rocks in ancient rocks or modern cores is most commonly done through drawings called graphical core logs (Bouma, 1962). These logs comprise a horizontal axis of grain size and a vertical axis of core depth. Annotated comments can then be added to the pictorial description. A full key to the symbols used during Expedition 340 is provided in Figure F2.

Graphical core logs were used during Expedition 340 because it is much quicker to draw the sequence of deposits than write a text description (and then enter that text via tabs or drop-down menus, as in DESClogik). The second reason for using graphical core logs is that it is easier for a reader to understand a picture than dense text. Graphical core logs have been widely employed over many decades (e.g., Bouma, 1962). DESClogik imposes predefined categories on users and necessitates placement of sharp boundaries between unit descriptions. Visual core logging, as completed during this expedition, allows a drawing of the core with minimal interpretation. It also allows more (necessary) flexibility in allowing the key to evolve and grow as observations of the cores are made. DESClogik requires a format and key to be defined before the cores are seen.

Grain size

Matrix grain size was estimated using a comparator card, which allows the describer to compare the core grain size to reference sizes on the card. The grain size categories used were mud (silt grains were not visible), muddy silt, <125 µm, <187 µm, <250 µm, <375 µm, <500 µm, <1 mm, <2 mm, <1 cm, and <10 cm. The use of grain size comparators ensures that the grain size estimated is the coarser tail of the grain size distribution (e.g., about the 95th percentile of the full distribution; Talling et al., 2004). The maximum and average size of clasts was noted in a separate column.

Boundaries and grading patterns

On the graphical core logs, sharp boundaries are denoted by a half arrow, and gradational boundaries are shown by triangles whose rotation shows whether the interval is inversely or normally graded. Erosional boundaries are shown by an inclined wavy line (Fig. F2).

Annotated comments

Where appropriate, written annotations were added to the graphical core log to clarify key observations (e.g., clast types, sizes, and percentage abundance). These comments are separated from the drawn log, as they may also on occasion involve interpretation rather than observation (Fig. F2). Similarly, the left-hand column is used to define layers that are definitely turbidites (e.g., as shown by cross-bedding or other features), tephra (ash fall or distal turbidites), blocky volcanic debris avalanches, or deformed intervals of more bedded seafloor sediment. This latter division of landslide deposits follows that of Watt et al. (2012).

Microscopic visual core description

Thin sections

Thin section analyses of sampled hard rock clasts were used to complement and refine macroscopic core observations, and this information was added to the database through DESClogik. Samples that represented a new lithologic or textural type were selected for thin section preparation. Phenocryst assemblages (and their modal percentages and sizes), groundmass, and alteration phases were determined, and textural descriptions were constructed. Textures were defined at the microscopic scale according to the degree of crystallinity of the groundmass (holohyaline to holocrystalline). A visual estimate of the modal percent of the phenocrysts was made, average crystal size for each mineral phase was determined, and the mineral shape and mineral habit were also determined. The following textural terms were used to describe the habit of crystals: "euhedral," "subhedral," "anhedral," and "interstitial." Grain shape was divided into four classes:

1. Equant (aspect ratio = <1:2),
2. Subequant (aspect ratio = 1:2 to 1:3),
3. Tabular (aspect ratio = 1:3 to 1:5), and
4. Elongate (aspect ratio = >1:5).

All observations were entered into the LIMS database using the Expedition 340 DESClogik thin section template.

Smear slides

Smear slide information was also added to the database using DESClogik. Smear slides are useful for identifying and reporting basic sediment attributes (texture and composition) in soft sediment, but results are not quantitative. Similar to the procedure used during Expedition 330, we estimated the abundances of biogenic and volcaniclastic constituents with the help of a visual comparison chart (Wentworth, 1922). Descriptive results are tabulated as

visual percentage estimates in the LIMS database, with values grouped into the following broad range of categories:

D = dominant (>50%).
A = abundant (>20%–50%).
C = common (>5%–20%).
P = present (>1%–5%).
R = rare (0.1%–1%).
T = trace (<0.1%).

Visual core descriptions

VCDs were generated from descriptive information retrieved from LIMS. VCDs combine key information input through DESClogik along with physical properties measurements (e.g., Fig. F4):

- Depth in meters below seafloor (mbsf),
- Scale for core section length,
- Sample piece number,
- Symbolized drilling disturbance intensity,
- Scanned digital image of the archive half,
- Lithologic unit number,
- Line chart displaying drilling disturbance by degree (slight, moderate, extreme, or none),
- Stacked line chart displaying clast composition and percentage (pumice, scoria, massive lava, vesicular lava, reworked [volcaniclastic], limestone [sedimentary], or other),
- Line chart displaying total clast content (1%–100%),
- Symbolized structural information,
- Structural measurements of dip direction and dip angle,
- Line chart displaying matrix alteration intensity (fresh [<2%], slight to moderate [2%–10%], moderate to high [10%–50%], or high to complete [50%–100%]),
- Sample type and position of intervals selected for different types of shipboard analytical studies,
- Neutron density, and
- Magnetic susceptibility.

Graphical core logs (see "Graphical core logs") drawn on board the research vessel were scanned and added as PDFs in a final column within the VCDs (Fig. F4). This strategy was adopted to combine the advantages of the graphical core logging approach and the data entry system via DESClogik.

Paleontology and biostratigraphy

During Expedition 340, preliminary age assignments were based on biostratigraphic analyses of calcareous nannofossils and planktonic and benthic foraminifers from core catcher samples. At appropriate intervals, additional nannofossil samples were collected in sections requiring a more refined age determination. Paleodepth interpretations were based on the paleoenvironmental requirements of cosmopolitan benthic foraminifers. Biostratigraphic calibrations (Wade et al., 2011; Kameo and Bralower, 2000) were correlated to the geomagnetic polarity timescale (GPTS) of Cande and Kent (1995) to be consistent with the methods described in "Paleomagnetism." Shipboard methods used to analyze and assess each microfossil group are detailed below.

Calcareous nannofossils

The calcareous nannofossil schemes of Okada and Bukry (1980) and Gartner (1977) were applied for the Neogene and Quaternary sequences, respectively. For the Quaternary sequences, the zonation of Gartner (1977) provides better resolution because of the use of the acme of small *Gephyrocapsa* sp. as a datum. For Zone CN14a, the species *Emiliania ovata* was considered to be *Pseudoemiliania lacunosa*, based on the discussion of Gartner (1977). Caribbean specific age calibrations (Table T1) for each zone were taken from Kameo and Bralower (2000).

Core catcher samples were prepared according to standard smear slide preparation techniques for examination with a light-polarizing microscope at 788× and 1250× magnification. A small amount of sediment was placed onto a coverslip with two drops of deionized water and smeared with a wooden toothpick. Norland optical adhesive was used to mount the samples, which were set to harden under an ultraviolet lamp for 10 min.

The overall preservation of each sample is evaluated in the following manner:

G = good; specimens show little or no evidence of dissolution.
M = moderate; specimens show some etching and/or recrystallization.
P = poor; specimens are severely etched or overgrown.

The relative abundance of individual species proposed by Hay (1970) was used:

HA = highly abundant; >100 specimens/field of view (FOV).
VA = very abundant; 11–100 specimens/FOV.
A = abundant; 1–10 specimens/FOV.
C = common; 1 specimen/2–10 FOV.
F = few; 1 specimen/11–100 FOV.
R = rare; 1 specimen/101–1000 FOV.
B = barren; no specimens.

Foraminifers

Biostratigraphic interpretations of planktonic foraminifers are based on the revised Cenozoic Tropical bioevents of Wade et al. (2011) (Table T2), specifically using those correlated to the GPTS of Cande and Kent (1995). Neogene planktonic foraminiferal taxonomy largely follows that of Kennett and Srinivasan (1983). For benthic foraminiferal taxonomic identification, the Ellis and Messina online catalogue (Ellis and Messina, 1940), Barker (1961), Poag (1981), Hayward and Kawagata (2005), and the generic classification scheme of Loeblich and Tappan (1988) were used. Paleodepth estimates were determined using depth ranges presented by Poag (1981) and Galluzzo et al. (1990).

Paleodepth nomenclature follows that of van Morkhoven et al. (1986):

Neritic = <200 m.
Bathyal = 200–2000 m.
Abyssal = >2000 m.

For each core catcher sample, ~10 cm³ of sediment was processed for planktonic and benthic foraminifer analysis. All samples were first disaggregated with water and washed over a 63 µm sieve. Highly indurated samples were soaked in a solution of 30% hydrogen peroxide until washed over a 63 µm sieve. The >63 µm sediment fraction was then dried in an oven at ~60°C until dry and then split for separate benthic and planktonic foraminiferal analyses. The <63 µm sediment fraction was not retained. To minimize contamination of foraminifers between samples, sieves were briefly soaked in methylene blue stain to identify any trapped foraminifers. Sieves were also occasionally ultrasonicated. Faunal analysis was carried out using either a Zeiss Stemi SV11 or Zeiss Discovery V8 binocular microscope. Analysis of benthic and planktonic foraminifers was based on the >150 µm fractions. For benthic foraminifers, up to 125 specimens per 1 gram of sample were picked. The >63 µm fraction was analyzed for a few select samples to provide a better representation of the breadth of benthic foraminiferal diversity. Preservation, abundance, and faunal composition data were also collected.

Planktonic foraminiferal preservation is categorized as follows:

VG = very good; no breakage or dissolution.
G = good; only very minor dissolution and no recrystallization; <10% of specimens are broken.
M = moderate; frequent etching and partial breakage; 30%–90% of specimens are unbroken.
P = poor; much dissolution and recrystallization; broken specimens dominate.

Benthic foraminiferal preservation is categorized as follows:

VG = very good; no evidence of overgrowth, dissolution, or abrasion.
G = good; little evidence of overgrowth, dissolution, or abrasion.
M = moderate; calcite overgrowth, dissolution, or abrasion are common but minor.
P = substantial overgrowth or infilling, dissolution, or fragmentation.

Planktonic foraminiferal abundance in relation to the total residue in the >150 µm fraction is defined as follows:

D = dominant; >30%.
A = abundant; >10%–30%.
F = few; >5%–10%.
R = rare; 1%–5%.
P = present; <1%.
B = barren; no planktonic foraminifers are present.

Benthic foraminifer abundance in relation to the total residue in the >150 µm fraction is defined as follows:

D = dominant; >30 specimens.
A = abundant; >10–30 specimens.
F = few; >5–10 specimens.
R = rare; >1–5 specimens.
P = present; 1 specimen.
B = barren; no benthic foraminifers present.

Geochemistry
Interstitial water collection

In general we attempted to take one or two samples from each 10 m core for pore water analyses; however, many of the collected cores were deemed inappropriate for pore water sampling because of sediment lithology (e.g., sand, debris, etc.). Pore fluid samples were extracted by squeezing whole-round sections. Once the core was on the catwalk, a 10–15 cm length of whole-round core was cut from the end of one to two sections per core. The whole rounds were transferred to the chemistry laboratory for squeezing. Whole-round sections were processed in a nitrogen-filled glove bag for sediment transfer into the squeezing apparatus. A hydraulic press was then used to squeeze the fluids from the sediment (e.g., Manheim, 1966). During squeezing, pore fluid was passed though one or two paper filters placed over titanium support screens. Following extraction, pore fluids were filtered through 0.5 µm syringe filters into various sample containers. Samples for inductively coupled plasma–optical emission spectrometry (ICP-OES) were acidified by adding ~10 µL of trace metal grade HNO_3. In addition to the standard shipboard

analyses (below), additional subsamples were collected as available water allowed. These samples were likewise acidified for shore-based analyses with Optima Grade HCl.

Interstitial water analysis

Salinity was estimated by measuring the sample refractive index. This measurement was done following sample processing on a ~100 µL sample using an Index Instruments Limited digital refractometer or by a handheld refractometer. In general, these two approaches appeared comparable. International Association for the Physical Sciences of the Oceans (IAPSO) standard seawater salinity values from both techniques yielded a value of 37 ppt, and there is a reasonable uncertainty of ±1 ppt for the handheld refractometer. Given these uncertainties, salinity data should be treated with caution. pH was measured with a combination glass electrode immediately prior to performing the alkalinity titration, and alkalinity was measured via Gran titration using a Metrohm autotitrator on ~3 mL of sample.

Sulfate, Cl, Mg, Ca, K, and Na were measured at sea using a Dionex ICS-3000 ion chromatography system. However, we do not report those data in this report, as the instrumentation produced highly erratic results. Figure F5 provides two comparison profiles of the shipboard and shore-based data. Although not all data exhibit this level of disagreement, these profiles demonstrate the general symptom that the shipboard data were less precise. The shore-based results presented here for total sulfur (ΣS), Na, Mg, Ca, and K were analyzed at Oregon State University. Instrumentation used was a Leeman Labs Prodigy ICP-OES. Emission lines were measured in radial view for all elements with the exception of ΣS, which was analyzed in axial mode. It is worth noting that the ICP sulfur measurement is not strictly speaking sulfate, as this instrumentation does not discriminate among the different species. However, for practical purposes, the dominant S species in the majority of our samples is sulfate. Thus, for clarity we refer to the ICP sulfur determination as ΣS. Reported uncertainties for the major cations and ΣS are derived in one of three ways. The first method utilizes (1) the regression uncertainty, which is calculated as the regression standard error, and (2) the uncertainty calculated from the standard deviation of three replicate analyses from each sample tube. These two factors are combined as the square root of the sum of squares. For the second and third assessments of uncertainty, we report the mean and standard deviation of a set of samples that were run either on the same or separate days. Samples using these latter two assessments are identified as such within the individual site pore fluid data tables. We note that the coefficient of variation for these analyses typically lies between ~1% and 2% for each of the major cations reported here, which is somewhat higher than our other measures of precision. For Sample 340-U1395B-10H-2, the duplicate run produced particularly high values for each of the analytes, and we suspect that the second analysis may have suffered from sample evaporation and the reanalyzed value is not included in our analyses here. To further assess precision, we also ran a set of IAPSO samples as unknowns. For 21 determinations (over three separate run dates), the mean and 1σ standard deviation for Na = 467.5 ± 2.5 mM, Mg = 53.8 ± 0.3 mM, K = 10.0 ± 0.1 mM, Ca = 10.4 ± 0.1 mM, and ΣS = 28.4 ± 0.3 mM. Chloride data reported here were analyzed on board the ship by the silver nitrate titration method using IAPSO standard seawater as a quality control reference. Dissolved ammonium was measured using standard colorimetric methods (Gieskes et al., 1991) on an Agilent Technologies Cary Series ultraviolet/visible light spectrophotometer.

Solid-phase geochemistry

For solid-phase analyses, a 5 cm³ plug sample was taken for carbonate, carbon-hydrogen-nitrogen analyzer (CHN), and XRD analyses. Samples were freeze-dried for ~24 h and ground by hand using an agate mortar and pestle in preparation for solid-phase analyses.

Inorganic carbon concentrations were determined using a Coulometrics Inc. CO_2 coulometer. Approximately 10–100 mg of dried, ground sediment was reacted with 2 M HCl, and the liberated CO_2 was titrated to an end point determined using a photodetection cell. $CaCO_3$ weight percentage was calculated from the inorganic carbon content, assuming that all evolved CO_2 was derived from calcium carbonate as follows:

$$CaCO_3 \text{ (wt\%)} = 8.33 \times IC \text{ (wt\%)},$$

where IC = inorganic carbon. This approach does not discriminate among carbonate minerals; thus, all the evolved CO_2 is treated as though it is derived from $CaCO_3$.

Total carbon and nitrogen were determined using a ThermoElectron Corporation FlashEA 1112 CHNS elemental analyzer with calibration using the Thermo Soil Reference Material NC standard (338 40025 Lot N12A). Sample analyses were performed on ~10–20 mg of dried, ground sediment. Total organic carbon content was estimated as the difference between inorganic carbon and total carbon.

XRD analyses were done using a Bruker D-4 Endeavor diffractometer with a Vantec-1 detector using

Ni-filtered CuKα radiation. Rapid mineral identifications (e.g., carbonates, hydrothermal alteration minerals, magmatic silicates, and oxides) were performed using EVA 13 software (Diffrac *plus* evaluation package). For Expedition 340 the generator voltage was 35 kV with a generator current of 40 mA. The scan was continuous from 4° to 70°2θ with a step size of 0.0174°, scan speed of 1 s/step, and a divergence slit of 0.6 mm. Mineral identification was performed using EVA software, with complementary mineral identification then performed using the Mineral Library of EVA Software.

Four main types of mineralogical associations were defined on the basis of XRD observations, and reference spectra given in Figure F6, F7, and F8 were used to rapidly investigate the data set. The first is a carbonate type (Type I) with minor or no volcanic minerals (Fig. F6). This type mainly consists of calcite and Mg-rich calcite with the possibility of some aragonite. Relative abundances of the different carbonates may be directly estimated from the 30°–40°2θ zone of the spectra (Fig. F9). Clay minerals (smectites, kaolinite, and glauconite) are often present in low amounts (mainly represented as bulges at low 2θ values). Illite and chlorite were not identified in the collected samples. The second is a volcanic type (Type II) with minor carbonate components (Fig. F7). This type contains plagioclase, amphibole (Hb), and pyroxenes (mainly orthopyroxene). Sometimes plagioclase is present alone. Quartz is a ubiquitous mineral phase in Sites U1397–U1400 but is absent in Sites U1393–U1396. A mixed type of mineral association (Type III, not represented) is a mixture of the previous types that were present in similar amounts. Finally, a clay minerals type (Type IV) is relatively rare and consists of the dominant clay minerals smectite, kaolinite, glauconite, and rarely halloysite or dolomite (Fig. F8). Also of note were numerous mineral phases such as orthopyroxene, pyrite, and Fe-Ti oxides, present in significant amounts as evidenced by visual observations, which are difficult to identify in the general spectra overview and necessitate longer investigations for identification in XRD spectra.

Microbiological sampling

Microbiological samples were only taken at Sites U1394–U1396 for shore-based analyses. The Operations Superintendent was notified prior to the intent to take microbiological samples, and a bag of fluorescent microspheres was added to the core barrel. As the APC was advanced, the bag burst and the microspheres were carried around the margins of the sediment core by circulating surface seawater. The penetration distance of microspheres into the interior portions of the core provided a measure of potential contamination by seawater prokaryotes (House et al., 2003).

Approximately nine microbiology samples were taken from each of these three sites. A 10 cm section of whole-round core was transferred to the N_2 bag for sampling. The exposed end of the core was scraped away using a sterile sampling spatula. A total of 3–4 cm³ of core material from the center of the core was then transferred to a sterile centrifuge tube and stored in the –80°C freezer. A further 20 cm³ of sediment was taken from the center of the core and transferred to Pyrex bottles and sealed with a rubber stopper. These samples were stored in a cold room or refrigerator at 0°C. Approximately 3–4 cm³ of sediment was also placed in a centrifuge tube for complementary geochemical analyses to the microbiology.

Headspace hydrocarbon gases

We analyzed one sample per core for headspace hydrocarbon gases as part of standard IODP shipboard safety monitoring (Kvenvolden and McDonald, 1986). For these analyses a ~3–5 cm³ sample was collected after the core was brought on deck. This sample was typically extracted from the exposed end of Section 1 of each core. The sample was placed into a 20 mL glass vial, which was in turn placed in an oven at 70°C for 30 min. Hydrocarbon gases (C1–C3) were analyzed using an Agilent/<HP> 6890 Series II gas chromatograph (GC3) equipped with a flame ionization detector at 250°C. The column was a 2.4 m × 3.2 mm stainless steel column packed with 100/120 mesh HayeSep R.

Physical properties

Physical properties measurements on sediment cores provide information that assists in the characterization of lithological units, stratigraphic correlation, heat flow, fluid flow, and consolidation history. They also help with the interpretation of seismic reflection profiles and downhole geophysical logging data. The primary objectives of the Expedition 340 physical properties program were to collect high-resolution data that (1) facilitate differentiation between mass transport events and background marine sedimentation; (2) constrain geothermal, geomechanical, and seismic properties; and (3) construct composite stratigraphic correlations.

We first measured physical properties on whole-round core sections using the Whole-Round Multisensor Logger (WRMSL), Natural Gamma Radiation Logger (NGRL), and thermal conductivity needle probe. Shear strength was measured on the core deck with a handheld penetrometer. We then split cores and

measured shear strength, *P*-wave velocity, and moisture content and density on the working half of the cores. The archive half was subsequently imaged with the SHIL and then analyzed for color reflectance and point magnetic susceptibility using the SHMSL. A full discussion of all methodologies and calculations (except the NGRL) used in the *JOIDES Resolution* physical properties laboratory can be found in Blum (1997).

Whole-Round Multisensor Logger measurements

Compressional wave velocity (on the *P*-wave logger [PWL]), gamma ray attenuation (GRA), and magnetic susceptibility were measured with the WRMSL followed by natural gamma radiation with the NGRL. These measurements are all nonintrusive and nondestructive.

The sampling interval for all WRMSL measurements was 2.5 cm, with an integration time of ~8 s for each measurement. We assessed the reliability of WRMSL measurements with standards every 2–12 h.

The core liner was assumed to be completely full. The bulk density values obtained from the GRA, along with the magnetic susceptibility measurements, underestimate true values if the liner is not completely full. The liners were not completely full for most sections cored with the XCB. Partially filled core liners also sometimes occurred when the recovered material was sand rich. Anomalously low *P*-wave velocity and density values also occur where there are cracks and gaps in the core. To limit data manipulation, we left anomalous values in the raw data. When plotting data and using data for correlation, we removed data from within 5.1 cm of each end to avoid end effects.

Gamma ray attenuation bulk density

Bulk density is calculated by measuring the attenuation of gamma rays as they pass through the core. Attenuation of these rays is dominated by Compton scattering and depends on the density and thickness of the sample. Gamma rays with an energy of 0.662 MeV are generated by a ^{137}Cs source core (Evans, 1965; Harms and Choquette, 1965) and pass through the entire diameter of the core. The GRA detector records these gamma rays on a 75 mm × 75 mm sodium iodide detector. The spatial resolution of the GRA is <1 cm.

Bulk density (ρ) is proportional to the gamma ray count,

$$\rho = 1/(\mu d) \times \ln (I_0/I),$$

where

μ = Compton attenuation coefficient,
d = sample diameter,
I_0 = gamma ray source intensity, and
I = measured intensity of gamma rays passing through the sample.

μ and I_0 are treated as constants obtained by calibrating the gamma ray detector with a set of aligned aluminum cylinders of various diameters surrounded by distilled water in a sealed core liner that is the same as that used during coring operations. The relationship between *I*, μ, and *d* is

$$\ln (I) = A(\mu d)^2 + B(\mathrm{m}d) + C,$$

where *A*, *B*, and *C* are coefficients obtained from the calibration. Gamma ray counts through each cylinder were determined for a period of 60 s. The bulk density of each aluminum cylinder was 2.7 g/cm³, and *d* was 1, 2, 3, 4, 5, or 6 cm.

Drift was assessed by running water standards every few hours. Calibration was performed at least twice per day and was always performed if deviations from the standard exceeded 2%.

Magnetic susceptibility

Magnetic susceptibility measures the ability of a material to be magnetized by an external magnetic field. The dimensionless volume magnetic susceptibility (κ) is defined as

$$\kappa = M/H,$$

where *M* is the magnetization induced by a field of strength (*H*). Magnetic susceptibility is primarily sensitive to the concentration of ferrimagnetic minerals (e.g., magnetite and maghemite). It is also sensitive to magnetic mineralogy and can be related to the origin of the materials in the core and their subsequent diagenesis. Igneous materials typically have magnetic susceptibility a couple of orders of magnitude greater than their alteration products, such as clay.

The WRMSL includes a Bartington Instruments MS2 and MS2C sensor coil operating at a frequency of 565 Hz. Because the core has a smaller diameter (66 mm) than the instrument aperture (88 mm), a volume correction must be made offline. For a core diameter of 66 mm and coil aperture of 88 mm, instrument measurements must be multiplied by a factor of 0.68 (Blum, 1997).

The calibration of the instrument is preset. Reliability of measurements was assessed prior to making any measurements by measuring κ on a 40 cm long piece of core liner filled with a mixture of magnetite

and epoxy and ensuring that the accuracy is within 5%. Every 2–6 h, water standards were analyzed to ensure there was no drift in the measurements. Spatial resolution is 4 cm based on the response function of the instrument. If the core is not continuous over an interval >8 cm, κ will be underestimated; such data is evident at the ends of cores because of these volumetric edge effects. Anomalous measurements were not removed from the raw data.

Compressional wave velocity

The PWL measures the traveltime of 500 kHz ultrasonic waves horizontally across the core at 2.5 cm intervals while it remains in the core liner. Waves are transmitted to the core by plastic transducer contacts connected to linear actuators. Pressure is applied to the actuators to ensure coupling between the transducers and the core liner.

P-wave velocity (*V*) is calculated by

$$V = d/t,$$

where *d* is the path length of the wave through the core and *t* is the traveltime. The total traveltime between the transducers includes the time delay related to transducer faces and electronic circuitry, the delay in the peak detection procedure, and the transit time through the core liner.

Traveltime is calculated by automated signal processing that detects the arrival of *P*-wave signals to a precision of 50 ns. The search method skips the first positive amplitude and finds the second positive amplitude using a detection threshold limit, typically set to 30% of the maximum amplitude of the signal. It then finds the preceding zero crossing and subtracts one wave period to determine the first arrival. To avoid extremely weak signals, minimum signal strength can be set (typically 0.02 V) and weaker signals are ignored. To avoid signal interference at the beginning of the record from the receiver, a delay (typically 0.01 ms) can be set to force the amplitude search to begin in the quiet interval preceding the first arrival. In addition, a trigger (typically 4 V) is selected to initiate the arrival search process, and the number of waveforms to be stacked (typically five) can also be set. A linear variable differential transformer (LVDT) measures the separation of the transducer to derive a signal path length (i.e., the core diameter). *P*-wave velocity is finally calculated after correction for system propagation delay, liner thickness, and liner material velocity.

The system is calibrated with a set of plastic cylinders with a range of diameters. Water standards were run every few hours to ensure measurements remained reliable. PWL velocities always remained within 2% of the room temperature value.

Natural gamma radiation logger measurements

Gamma rays are emitted from decay of 238-uranium (^{238}U), 232-thorium (^{232}Th), and 40-potassium (^{40}K). The NGRL measures this natural emission on whole-round cores using a system designed and built at IODP-USIO (Texas A&M University, USA) between 2006 and 2008 (Vasiliev et al., 2011). This system has been used on every IODP-USIO expedition starting with Expedition 320.

The NGRL contains eight NaI scintillator detectors, seven plastic scintillator detectors, and 22 photomultipliers. NaI detectors are covered by 8 cm of lead for passive shielding. Half of the lead shielding closest to the NaI detectors is composed of low-background lead, and the outer half is composed of regular (virgin) lead. NaI detectors are separated by 7 cm of low-background lead. The NGRL uses a plastic scintillator to suppress high-energy gamma and muon components of cosmic radiation by producing a canceling signal when these charged particles pass through the plastic scintillators. The NGRL was calibrated with ^{137}Cs and ^{60}Co sources and identifying peaks at 662 keV (^{137}Cs) and 1330 keV (^{60}Co) using the 1170 keV peak for verification. Calibration materials were provided by Eckert & Ziegler Isotope Products Inc. (Valencia, California, USA).

Gamma ray counts are summed over the range of 100–3000 keV and are thus comparable with data collected during previous cruises and can be directly compared with downhole logging data. Background measurements over a 36,000 s time span were made on an empty core liner upon arrival at the first site and two other times during the expedition.

Characterization of each section consisted of eight measurements at two positions for a total of 16 measurements at 10 cm intervals. Spatial resolution, defined by the full width at half-maximum, is 19 cm. An edge correction was applied to measurements within 20 cm of the ends of each section (Vasiliev et al., 2011). The quality of the energy spectrum depends on the concentration of radionuclides in the sample, but also on the counting time, with higher times yielding better spectra. A previous study on pelagic sediments (very little gamma radiation activity) with minor amounts of siliciclastic material used the same apparatus; with counting times of 5 min at each position, spatial variations in natural gamma radiation (NGR) were identified reliably and used for stratigraphic correlation (Vasiliev et al., 2011). We thus used counting times of 5 min at each position to ensure reliable counting statistics. Measurements made at the ends of each section appear to be systematically lower than adjacent measurements, even after end corrections are made.

When plotting data and using NGR data for correlation, we discarded data from within 10 cm of both ends of the each section to avoid end effects.

Thermal conductivity measurements

Thermal conductivity measures the ability of a material to transfer heat by conduction. It is used, in combination with measurements of temperature, to calculate heat flow. Its value also depends on composition, porosity, and structure and thus complements other physical property measurements.

Thermal conductivity was measured with a TeKa TK04. All measurements were made after the core had equilibrated with the ambient temperature in the laboratory (>2.5 h) and after WRMSL and NGR measurements. A 2 mm hole for insertion of the probe was drilled into the side of the sample liner, typically close to the midpoint of the section. The measurement is reported at the location in the core. Prior to each measurement, thermal drift within the sample was measured to ensure that it would not significantly affect measurements (<0.04°C/min). Measurements were made once the thermal drift was stable, typically after 5 min. A calibrated heat source was then turned on and the increase in temperature was recorded over 90 s. A heating power of 2 W/m was typically used; large values produce greater signals but also promote undesirable processes such as convection in the pore fluids. The solution to the heat conduction equation with a line source of heat was then fit to the temperature measurements to obtain the thermal conductivity. Very high water content, inhomogeneous samples, and highly disturbed samples may cause deviations from the solution to the conduction equation. In the case of a poor fit, we did not keep the data.

Prior to measurements, a test was performed on a standard of MACOR plastic standard with

$$k = 1.626 \text{ W/(m·K)} \pm 2\%.$$

Measured values were within 3%. This test was typically performed once per day.

Reported data are not corrected to in situ conditions. The effect of increasing pressure is to increase thermal conductivity (k). The pressure correction is +1% for each 1800 m depth assuming a hydrostatic pressure gradient (Ratcliff, 1960). The effect of temperature is more complicated. The thermal conductivity of the matrix solids is inversely proportional to temperature (Zoth and Haenel, 1988). In contrast, the thermal conductivity of water increases with temperature (Keenan et al., 1978). The temperature correction for each +20°C change in temperature can be as high as +5% for a high-porosity, water-saturated

sediment (Ratcliff, 1960) and –3% for hard rocks (Clark, 1966). These corrections are similar to the TK04 measurement uncertainty, about 5% during routine evaluation.

Downhole temperature measurements

In Holes U1395–U1400, downhole temperature was measured using the APCT-3. This tool allows temperature to be measured while drilling. By shooting the tool forward ~9.5 m during coring, the thermal effects of drilling are minimized. The APCT-3 records temperature with a glass-encapsulated thermistor (Model YSI 55032) at the outside edge of the cutting shoe. Details of its calibration and testing are described by Heesemann et al. (2006). Temperature was recorded downhole for ~10 min (as short as 2 min and as long as 48 min) and sampled every 2 s. This is not long enough for the probe to thermally equilibrate with its surroundings. Consequently, the recorded evolution of temperature was fit to a theoretical solution to the temperature evolution using TP-Fit software (see APCT-3 user manual on the Cumulus/Techdoc database at **iodp.tamu.edu/tasapps/**). This theoretical solution assumes all heat transfer occurs by conduction and that we can neglect fluid flow induced by the insertion of the tool and convection driven by the large temperature gradients produced by friction. The calculated temperature depends on thermal conductivity, density, and the specific heat capacity of the surroundings. Uncertainty in these thermal properties dominates the uncertainty in the recovered temperature. Typical uncertainties on the best-fit temperature determined by TP-Fit are <0.08°C, assuming a 10% uncertainty on these material properties.

Temperature at the seafloor was also estimated from the coldest stable temperatures recorded at the mudline before the probe enters the hole. The probe typically sat at the mudline for 5 min.

Moisture and density measurements

Several basic properties of interest (water content, bulk density, dry density, porosity, and void ratio) are measured more accurately through mass and volume determinations on discrete samples. MAD data were used for comparison with GRA bulk density data from the WRMSL. The shipboard MAD facility on the *JOIDES Resolution* includes a dual balance system and a hexapycnometer.

During Expedition 340, only soft to weakly lithified sediments were cored. In undisturbed core, 1–2 MAD samples were collected close to XRD/carbonate samples. From APC cores, cylindrical MAD samples were taken with a syringe. In XCB cores, fragmented

domains, a result of the coring processes, were sampled with forceps in order to minimize further core damage.

Dual balance system

The dual balance system was used to measure both wet and dry masses. The two coupled analytical balances (Mettler-Toledo XS204) were used to compensate for ship motion, one acting as a reference and the other used for measurement of the unknown. Before weighing sample-standard pairs, the balances were "tared" to zero across 300 measurements. Standard weights of similar value to the sample weight were placed upon the reference balance and the sample was placed on the unknown balance. We took 300 measurements (taking ~1.5 min).

Wet and dry mass

Immediately after sediment samples were collected, we measured wet sediment mass (M_{wet}). Dry sediment mass (M_{dry}) and volume (V_{dry}) were measured after drying the samples in a convection oven for >24 h at a temperature of 105° ± 5°C. Dried samples were then cooled in desiccator for >1 h before the dry mass was measured. Dry volume was measured using a helium-displacement pycnometer with a nominal precision of ±0.04 cm³. Each reported value consists of an average of three measurements. It is recommended that for future projects, weighing of samples in the dual balance should be done with a plastic lid on the glass container in order to avoid moisture loss/gain during measurement. This requires that tare of the glass containers should be measured with their lids at IODP-USIO, prior to the cruise.

Hexapycnometer system

The hexapycnometer system measures dry sample volume using pressurized, helium-filled chambers. At the start of the expedition, and whenever the helium gas tank was changed, a calibration was performed using stainless steel spheres of known volume. A batch of samples consisted of five cells with unknowns and one cell with two stainless steel spheres (3 and 7 cm³). The spheres were cycled through the cells to identify any systematic error and/or instrument drift. After conducting 12 calibrations (two on each of the six cells) using these spheres, we calculated a mean error of 0.126%. Samples should be close to 10 cm³; the larger the sample the higher the precision of the method. Individual volume measurements were preceded by three purges of the sample chambers with research grade (99.995% or better) helium heated to 28°C, followed by three data acquisition cycles.

Final calculation

For calculation of sediment bulk density, dry density, grain density, porosity, and void ratio, we used the traditional ODP method ("Method C"; Blum, 1997). Water content, porosity, and void ratio are defined by the mass or volume of extracted water before and after the removal of interstitial pore water through the drying process. Standard seawater density (1.024 g/cm³) is used for the density of pore water and a standard salinity of 0.035 (s = S/1000; Blum, 1997).

Water content

Water content was determined following the methods of the American Society for Testing and Materials (ASTM) designation D2216 (ASTM International, 1990). Corrections are required for salt when measuring the water content of marine samples. Pore water salinities of 0.035 were used for all Expedition 340 samples. In addition to the recommended water content calculation in ASTM D2216 (i.e., the ratio of pore fluid mass to dry sediment mass [percent dry weight]), we also calculated the ratio of pore fluid mass to total sample mass (percent wet weight). Moisture content is pore water mass expressed either as percentage of wet bulk mass or the mass of salt-corrected solids:

$$W_c \text{ (% of mass of salt-corrected solids)} = (M_t - M_d)/(M_d - s{\cdot}M_t)$$

and

$$W_c \text{ (% of wet bulk mass)} = (M_t - M_d)/(1 - s)\,M_t,$$

where

M_t = total mass of the saturated sample,
M_d = mass of the dried sample, and
s　 = salinity.

Porosity, bulk density, and grain density

Porosity (φ) was calculated using

$$\varphi = (W_c \times \rho)/[(1 + W_c)\rho_w],$$

where

ρ　 = measured bulk density,
ρ_w = density of the pore fluid, and
W_c = water content expressed as a decimal ratio of percent dry weight.

Bulk density is the density of the saturated samples, with $\rho = M_t/V_t$. Mass (M_t) was measured using the balance, and volume (V_t) was determined from pycnometer measurements of grain volume and the

calculated volume of the pore fluid ($V_t = V_{pore} + V_d$). For lithified samples from Expedition 340, bulk density was determined directly from $\rho = M_t/V_t$.

Grain density (ρ_{grain}) of unconsolidated samples was determined from measurements of dry mass and dry volume made in the balance and the pycnometer, respectively. Mass and volume were corrected for salt using

$$\rho_{grain} = (M_d)/(V_t - V_{salt})$$

and

$$V_{salt} = [(M_t - M_d)s]/[(1 - s)/\rho_{salt}],$$

where s is the salt content (in grams) and ρ_{salt} is the density of salt (2.257 g/cm³).

Compressional wave velocity measurements

The measurement of compressional wave velocity was carried out on wet sediment on the working half of the split cores. Measurements were made in two orientations with caliper-type contact probe and bayonet transducers. Measurements perpendicular to the core (x-axis) were made on every section unless core quality was compromised. X-axis measurements could be performed in most core sections. The initial plan was to make measurements parallel to the core (z-axis) once per core. Because z-axis measurements could only be carried out in loose, coarse sediments where the bayonets could enter the split core without damaging the sediment structure, almost no sections were ammenable to this measurement. This measure was abandoned after Hole U1394B.

For more efficient contact, deionized water was applied on the lower transducer in contact with the core liner for the measure of the x-axis.

The system uses Panametrics-NDT Microscan delay line transducers with a frequency of 500 kHz. The distance between the two transducers was measured with a built-in LVDT. The P-wave passing through the sample was recorded, and we picked first arrivals as the initial rise of the first peak using an automated procedure. The measure along the x-axis included the core liner of known thickness.

A series of calibrated acrylic cylinders of known P-wave velocities (2750 ± 20 m/s) and thicknesses were used at least once a day for calibration. This calibration compared the acrylic cylinder thickness multiplied by the time to cross the cylinder with the known P-wave velocity.

We speculate that this method may result in slightly different P-wave velocities than the WRMSL because

transducers are in direct contact with the sediments and have better coupling.

Shear strength measurements

Shear strength is the resistance of a material to failure in shear. Shear stress in unconsolidated materials is resisted only by the skeleton of solid particles. Shear strength (τ_f) can be expressed as a function of the effective normal stress at failure (σ'), the effective cohesion (c'), and friction angle (ϕ'):

$$\tau_f = c' + \sigma' \tan \phi',$$

where c' and ϕ' are the shear strength parameters that define a linear relationship between τ_f and σ', according to the Mohr-Coulomb failure criterion.

Shear strength parameters can be determined by means of multiple laboratory tests. c' and ϕ' are relevant in situations where field drainage conditions correspond to test conditions. The shear strength of a soil under undrained conditions (pore fluid drainage does not occur during failure) is different from that under drained conditions (pore fluid drainage occurs).

Undrained shear strength can be expressed in terms of total stress in the case of fully saturated materials of low permeability (e.g., clays), denoted by S_u. The most common strength tests in shipboard laboratories are the vane shear and penetrometer tests, which provide measurement of undrained shear strength (S_u) (Blum, 1997). The fall cone test also provides a good estimate of S_u (Hansbo, 1957; Wood, 1985).

During Expedition 340, S_u was measured in undisturbed fine-grained sediments using a handheld penetrometer at the base of each core section and the automated vane shear (AVS) system and the fall cone in working-half cores. Shear strength measurements with the AVS and the fall cone were performed in the y–z plane, whereas measurements with the handheld penetrometer were performed in the y–x plane. Measurements performed with these three methods were performed rapidly to avoid draining and evaporation, in order to provide measures of undrained shear strength.

Automated vane shear system

Using the AVS, undrained shear strength was determined by inserting a four-bladed vane into the split core and rotating it at a constant 90°/min to determine the torque required to cause a cylindrical surface to be sheared by the vane, which provides a measurement of the peak shear strength. The difference in rotational strain between the top and the bottom of a linear spring is measured using digital shaft encoders. Measurements were made with the

vane rotation axis and penetrometer penetration direction perpendicular to the split surface. The residual shear strength was taken to be the constant and lowest measured shear strength after reaching the peak value during the test cycle. Sampling rates were one per core section unless the sediment was too firm for instrument penetration or was disturbed during coring.

Vane shear strength $S_{u(v)}$ (kPa) is calculated as

$$S_{u(v)} = T/K_v = (\Delta/B)/K,$$

where

T = torque required to induce material failure (N·m),
K_v = constant, depending on vane dimensions (m³),
Δ = maximum torque angle (°) at failure, and
B = spring constant that relates the deflection angle to the torque (°/N·m) (Blum, 1997).

All measurements used a vane with a height and diameter of 12.7 mm. Failure torque (T) was determined by measuring the degrees of rotation of one of four torsional springs. A linear calibration equation (specified by the manufacturer) relates the rotation angle to the torque for the particular spring being used. Selection of the appropriate spring was based on the anticipated shear strength of the material. Vane shear results were generally considered reliable for shear strength values less than ~150–200 kPa, above which excessive cracking and separation of the core material occurred.

Handheld penetrometer

A handheld penetrometer (Soiltest 29-3729) was used to obtain additional undrained shear strength measurements. A handheld penetrometer is a flat-footed, cylindrical probe that is pushed 6.3 mm into the base of sections on the catwalk that have not yet been split. The resulting resistance is the unconfined compressive strength (τ_f), which corresponds to twice the value of $S_{u\ PP}$, measured in kilograms per square centimeter. Therefore, undrained shear strength (in kPa) is obtained by

$$S_{u\ PP} = 98.1\ (\tau_f/2)^2.$$

Measurements using the handheld penetrometer were attempted once per core section at the base of the section if undisturbed soft fine-grained sediment was present. The handheld penetrometer can measure a maximum value of 220 kPa, a value that characterizes firm sediment.

Fall cone

The fall cone test is a standardized test method for liquid and plastic limit determination that can also be used for undrained shear strength measurements. During Expedition 340 it was used only for undrained shear strength measurements. The apparatus consists of a penetrometer fitted with a 35 mm long and 30° angle stainless steel cone; the cone and the sliding shaft to which it is attached have a combined mass of 80 g, resulting in a 0.785 N cone, according to the British Standard (British Standards Institution, 1990).

Measurements were performed by placing working-half core sections below the cone. The cone was lowered so that it just touched the surface of the soil in the cup. The cone was locked in its support at this stage. The cone was then released, and its depth of penetration into the material was measured. One fall cone measurement was performed on each core section, except in heterogeneous material, where the number of measurements was dictated by material changes.

A number of studies have found that undrained shear strength at the liquid limit ranges from 1.7 to 2.3 kPa. Hansbo (1957) proposes

$$S_{u\ FC} = k(W/d^2),$$

where

$S_{u\ FC}$ = undrained shear strength,
k = cone factor,
W = cone weight, and
d = cone penetration in intact soils.

For the cone used (30°/0.785N), the depth of penetration corresponding to the liquid limit is 20 mm. The cone factor k is 0.85 for a 30° cone (Wood, 1985).

Stratigraphic correlation

Stratigraphic correlation consists of identifying common strata between holes at a site. This identification is important for clarifying the stratigraphic relationship between holes. Strata have distinct geophysical signatures identifiable in physical properties measurements. Although holes at a site may be offset by only tens of meters from each other along the seafloor, variations in stratigraphic depth between holes can sometimes be several meters. Differences in stratigraphic depth result from variations in seafloor depth, sedimentation rates, faulting or erosion histories at each hole. Small differences may arise from disruption of sediment during coring and recovery. Therefore, it is necessary to adjust the depth of core data between holes to ensure proper comparison of stratigraphic boundaries. It was sometimes difficult in this study to conduct stratigraphic correlations because of the complex nature of the sediment. The thickness and character of sediment in submarine slides and debris avalanches can have significant

spatial variability over short distances, and it is possible that strata in one hole may not exist in another. We conducted only broad, first-order correlations during Expedition 340 that tie only clear and consistent changes in physical properties between holes.

Initial stratigraphic correlations between holes drilled at each site were generated using Analyseries software. Analyseries is freeware that runs on Macintosh computers, so adjustments and corrections to all stratigraphic correlations can be made by scientists postcruise as needed by downloading this software and the raw data files (**www.ncdc.noaa.gov/paleo/softlib/softlib.html**). Analyseries provides linear depth adjustment between a reference hole and adjacent holes at the same site and calculates correlation coefficients for all depth adjustments. This is not the same procedure as that performed by the CoreWall correlator software commonly used during IODP expeditions to create meters composite depth (mcd) scales and calculate associated growth factors. As such, the correlated data cannot be considered composite depths, but they do allow for first order comparisons between holes. We typically used the hole with the most complete core recovery as the reference hole. Bulk density, magnetic susceptibility, and *P*-wave velocities measured with the multisensor loggers and NGR measured with the NGRL were all used to make stratigraphic correlations. Bulk density and magnetic susceptibility usually provided the most robust correlation tie points, although NGR was also a useful data set for checking correlations. Although only physical properties were used to generate the correlations, the final correlations were compared with the core descriptions. We conducted stratigraphic correlation only after core recovery was completed at a site. The analysis involved visually selecting signals that appeared consistently in both the reference and comparison holes. Tie points were first made using magnetic susceptibility, followed by bulk density, and if needed, NGR and *P*-wave data sets. To ensure consistency, tie points using one data set were compared to tie points picked with other data sets. After picking tie points, we generated correlation coefficients (*R*) between the two holes, and from this determined the quality of the fit. The correlation coefficient can range from –1 (exactly anticorrelated) to 1 (exactly correlated). The correlation coefficient calculation in Analyseries does not automatically remove data gaps. If large data gaps exist, correlations can therefore be anomalously low. During the picking process, we updated the correlation coefficient to ensure that *R* values improved for all of the data sets used in the correlation, regardless of which data set was used to make the tie point. It is important to note that only clearly defined correlation points associated with strong peaks and troughs are used for this initial run.

Linear interpolations stretch and squeeze the stratigraphic record rather than hanging the data next to each other as in the CoreWall correlator software. More detailed correlations should be made postcruise, especially if sites require construction of a mcd scale.

Paleomagnetism

Samples, instruments, and measurements

Paleomagnetic investigations during Expedition 340 were focused on measurement of the NRM of archive-half sections before and after alternating field demagnetization. NRM measurements of entire split archive-half sections were made using a 2G Enterprises model 760R SRM optimized for IODP section halves (15.59 cm^2 cross-sectional area), equipped with superconducting quantum interference devices (SQUIDs) and an in-line automated alternating field demagnetizer capable of reaching a peak field of 80 mT. The SRM generates measurements of magnetic inclination, declination, and intensity for each measurement interval.

With *x*-, *y*-, and *z*-axis pickup coil response functions of 6.1, 6.2, and 9.9 cm, respectively, the measured area at each programmed interval is integrated over ~100 cm^3 (Richter et al., 2007). Measurement of an empty tray followed by correction for background drift allows for estimation of the ambient noise level at ~2 × 10^{-6} A/m. Thus, for split-core samples, the minimum measurable intensities of the SRM are around one order of magnitude greater, or ~2 × 10^{-5} A/m.

NRM was measured continuously at 2.5 cm intervals along the archive-half sections. This spacing was agreed on by the physical properties specialists and those describing the cores, ensuring coeval depth data were available for multiple properties. NRM measurements were also made over a 15 cm long interval before and after each core section. These measurements, referred to as header and trailer data, serve the dual function of monitoring the background magnetic moment and allowing for deconvolution of the response function of the pickup coils. Typically, NRM was measured before and after AF demagnetization in a peak field of 20 mT, with an additional step at 10 mT (and sometimes 5 mT and 15 mT) when time and core flow allowed. With no onboard deconvolution, we removed measurements from the first and last 10 cm of each section before incorporation into figures, as these regions are most affected by volumetric edge effects associated with the response function of the instrument.

To provide a check on the SRM data and enable more detailed magnetic investigations, we sampled the working-half core sections with 8 cm^3 plastic cubes. Taken from the center of the working half, these dis-

crete samples are potentially less affected by several sources of magnetic overprint (Fuller et al., 2006; Richter et al., 2007). We measured the NRM of these samples on an Agico (JR-6A) dual-speed spinner magnetometer in six positions (sensitivity = ~2×10^{-6} A/m) and AF demagnetized them in fields of 5, 10, 15, and 20 mT using an ASC Scientific D-2000 AF demagnetizer. For some samples we demagnetized samples in fields as high as 60 mT in 5–10 mT steps above 20 mT, and in Hole U1398B we demagnetized three samples in a peak field of 100 mT. These three samples were also imparted with an anhysteretic remanent magnetization (ARM) (100 mT AF in a 0.05 mT direct current bias field) using the D-2000 demagnetizer, and an isothermal remanent magnetization (IRM) using an ASC Scientific IM-10 Impulse magnetizer in fields of 20, 100, 300 and 1000 mT. These induced magnetizations were used to create ratios to estimate magnetic grain size and magnetic mineralogy independent of the concentration of magnetic grains. Magnetic intensity and directional data for each discrete sample were interpreted through Zijderfeld diagrams and normalized demagnetization data to assess sediment coercivity and evidence for magnetic overprinting.

We did not demagnetize any split archive-half sections in fields >20 mT. This decision was taken with a view to preserve some of the NRM for postcruise analysis, where time allows for higher resolving measurements. A field of 20 mT was deemed sufficient to remove the drilling overprint when cores were retrieved using nonmagnetic core barrels.

Coring and core orientation

The standard IODP paleomagnetic coordinate system was used (Fig. F10; Richter et al., 2007). In this system, +x is perpendicular to the split core surface and upward out of the working half, +z is downcore, and +y is orthogonal to x and z in a righthand sense (i.e., left along the split-core surface when looking upcore at the archive half). Discrete samples were taken from the working half and oriented upcore (thus +z is downcore, +x is into the working half, and +y is to the right looking upcore); rotating these cubes through 180° around the z-axis ensured the coordinates were directly comparable to the archive half.

The FlexIt orientation tool can be deployed with APC cores using nonmagnetic barrels. The FlexIt tool uses three orthogonally mounted fluxgate magnetometers to record the declination, inclination, and total magnetic field of the core barrel relative to magnetic north immediately prior to firing. This data is in reference to the double lines scribed on the core liner; thus the extruded core can be azimuthally aligned with respect to magnetic north. FlexIt data

was acquired for all nonmagnetic barrel APC cores from Hole A and often acquired for Holes B and C. Site figures show uncorrected declination (gray) and, where available, true north–corrected declination (with FlexIt correction applied; red). For APC cores without Flexit data we use the discrete inclination data (SRM data from cores recovered using standard barrels often suffer a strong overprint) to determine polarity and guide declination rotation. These SRM sections can be rotated to a mean of true north for normal polarity intervals and rotated through 180° for periods of reversed polarity (orange data in figures). Because core rotation can occur during XCB coring, declination can suffer rifling through the entire core length. This effect is neither measurable nor easily predictable; thus, for all cores recovered with the XCB coring system declination remains uncorrected.

Magnetostratigraphy

Magnetostratigraphic interpretations of the paleomagnetic record will be restricted to intervals dominated by undisturbed hemipelagic sediment as these sequences are most likely to preserve reliable paleogeomagnetic information. Before interpretation for magnetostratigraphy, data were first assessed to determine if they could be used to interpret the behavior of the geomagnetic field. These criteria include assessment of the degree of magnetic overprinting through AF demagnetization of discrete samples, comparison of site inclination and declination data to those predicted by assuming a geocentric axial dipole (GAD), and replication of data between holes. For sites cored during Expedition 340, GAD inclination ranges from ± 31.0° (Site U1393) to ± 27.0° (Site U1398); the declination of all sites from true north is approximately –14°W. Data that satisfied these criteria were available to be used to create reversal based stratigraphies through comparison to a GPTS. We chose to employ the GPTS of Cande and Kent (1995) after discussions with biostratigraphers (Table T3). Polarity reversals are identified in our data as regions where inclination transitions between positive and negative values predicted by GAD, accompanied by a 180° shift in declination. The magnetostratigraphic ages for each site are constructed by correlating these transitions with their equivalent well-dated horizon in the GPTS. Reversals are not unique and transition from either normal to reversed polarity (or vice versa), thus a continuous record is often required to make a confident interpretation of magnetostratigraphy. Where this is not possible, biostratigraphic datums can be used in tandem with the paleomagnetic results to constrain and significantly limit the range of possible correlations with the GPTS. This proved critical for Expedition 340, as continuous records were not always obtainable.

Comparable depth scales

For Sites U1395 and U1396, paleomagnetic directions from different holes are compared on a common depth scale. This first-order common depth scale was created in the program Analyseries, primarily using magnetic susceptibility measured every 2.5 cm using a 80 mm Bartington MS2C loop. The least complete record is usually transferred to the hole with the most complete recovery. Although this cannot be considered a meters composite depth scale, it does allow measurements to be transferred between holes and construction of a preliminary site record. For a more complete explanation of this procedure, see "Physical properties."

Downhole logging

Downhole logs are measurements of physical, chemical, and structural properties of the formation surrounding a borehole that are made after completion of drilling. Data are continuous with depth (at vertical sampling intervals ranging from 2.5 mm to 15 cm) and are measured in situ. The sampling is intermediate between laboratory measurements on core samples and geophysical surveys and provides a necessary link for the integrated understanding of physical properties on all scales.

Logs can be interpreted in terms of the stratigraphy, lithology, mineralogy, and geochemical composition of the penetrated formation. They also provide information on the condition, shape, and size of the borehole and on possible deformations induced by drilling or formation stress. When core recovery is incomplete or disturbed, log data may provide the only way to characterize the formation. Data can be used to determine the actual thickness of individual units or lithologies when contacts are not recovered, to pinpoint the depth of features in cores with incomplete recovery, or to identify intervals that were not recovered.

Operations

Logs are recorded with a variety of tools combined into several tool strings, which are run down the hole after completion of drilling operations. Four tool strings planned for deployment were used during Expedition 340: a triple combination, or triple combo, string (spectral and natural gamma radiation, density, and resistivity); a modified triple combo string (spectral and natural gamma radiation, density, resistivity, and magnetic susceptibility); a Formation MicroScanner (FMS)-sonic string (gamma ray, sonic velocity, and resistivity images); and the Versatile Seismic Imager (VSI) string; vertical seismic profile and gamma ray) (Fig. F11; Table T4).

In preparation for logging, the boreholes were flushed of debris by circulating a "slug" of viscous drilling fluid (sepiolite mud mixed with seawater; approximate density = 8.8 ppg or 1.055 g/cm³; if barite-weighted, density = 10.5 ppg or 1.258 g/cm³) through the drill pipe to the bottom of the hole. The BHA was pulled up to ~80 mbsf. Tool strings were then lowered downhole by a seven-conductor wireline cable during sequential deployments. Each tool string deployment is a logging "run," starting with the assembly of the tool string and the necessary calibrations. The tool string is then sent down to the bottom of the hole while recording a partial set of data and, except for the VSI, is pulled up at a constant speed, typically 250–500 m/h, to record the main data. The VSI is held stationary at regularly spaced depths while shooting the seismic source and then pulled up between stations. During each run, tool strings can be lowered down and pulled up the hole several times for control of repeatability or to try to improve the quality of the data. Each lowering or raising of the tool string while collecting data constitutes a "pass." During each pass, incoming data are recorded and monitored in real time on the surface MCM MAXIS system. A logging run is complete once the tool string has been brought to the rig floor and disassembled. A wireline heave compensator (WHC) was employed to minimize the effect of ship's heave on the tool string's position in the borehole (see "Wireline heave compensator").

Logged properties and tool measurement principles

The main logs recorded during Expedition 340 are listed in Table T5. More detailed information on individual tools and their geological applications may be found in Ellis and Singer (2007), Goldberg (1997), Lovell et al. (1998), Rider (1996), Schlumberger (1989), and Serra (1984, 1986, 1989). A complete list of acronyms for the Schlumberger tools and measurement curves is available at www.apps.slb.com/cmd/.

Natural radioactivity

The Hostile Environment Natural Gamma Ray Sonde (HNGS) was used on the triple combo tool string to measure natural radioactivity in the formation. It uses two bismuth germanate scintillation detectors and five-window spectroscopy to determine concentrations of K, Th, and U. The radioactive isotopes of these three elements dominate the natural radiation spectrum. The HNGS filters out gamma ray energies below 500 keV, eliminating sensitivity to bentonite or KCl in the drilling mud and improving measurement accuracy.

The Enhanced Digital Telemetry Cartridge (EDTC; see "Telemetry cartridges"), which is used primarily to communicate data to the surface, includes a sodium iodide scintillation detector to measure the total natural gamma ray emission. The EDTC is not a spectral tool, but it provides high-resolution total gamma ray for each pass, which allows for precise depth match processing between logging runs and passes.

Density

Formation density was measured with the Hostile Environment Litho-Density Sonde (HLDS). The sonde contains a radioactive cesium (^{137}Cs) gamma ray source (622 keV) and far and near gamma ray detectors mounted on a shielded skid, which is pressed against the borehole wall by an eccentralizing arm. Gamma rays emitted by the source undergo Compton scattering, where gamma rays are scattered by electrons in the formation. The number of scattered gamma rays that reach the detectors is proportional to the density of electrons in the formation, which is in turn related to bulk density. Porosity may also be derived from this bulk density if the matrix (grain) density is known. Good contact between the tool and borehole wall is essential for good HLDS logs; poor contact results in underestimation of density values.

The HLDS also measures photoelectric absorption as the photoelectric effect (PEF). Photoelectric absorption of the gamma rays occurs when their energy is reduced below 150 keV after being repeatedly scattered by electrons in the formation. Because PEF depends on the atomic number of the elements encountered, it varies with the chemical composition of the minerals present and can be used for the identification of some minerals. For example, the PEF of calcite is 5.08 b/e⁻ and the PEF of quartz is 1.81 b/e⁻.

Electrical resistivity

The High-Resolution Laterolog Array (HRLA) provides six resistivity measurements with different depths of investigation (including the borehole, or mud resistivity, and five measurements of formation resistivity with increasing penetration into the formation). The tool sends a focused current beam into the formation and measures the intensity necessary to maintain a constant drop in voltage across a fixed interval, providing direct resistivity measurement. The array has one central (source) electrode and six electrodes above and below it, which serve alternately as focusing and returning current electrodes. By rapidly changing the role of these electrodes, a simultaneous resistivity measurement at six penetration depths is achieved. The tool is designed to ensure that all signals are measured at exactly the same time and same

tool position and to reduce the sensitivity to shoulder bed effects. Typically, igneous minerals found in crustal rocks, calcite, silica, and hydrocarbons are electrical insulators, whereas ionic solutions like pore water are conductors. Electrical resistivity, therefore, can be used to evaluate porosity (via Archie's law) for a given salinity and resistivity of the pore water.

Magnetic Susceptibility Sonde

The Magnetic Susceptibility Sonde (MSS), a wireline tool designed by the Lamont-Doherty Earth Observatory (LDEO), measures the ease with which formations are magnetized when subjected to Earth's magnetic field. The ease of magnetization is ultimately related to the concentration and composition (size, shape, and mineralogy) of magnetizable material within the formation. This measurement provides one of the best methods for investigating stratigraphic changes in mineralogy and lithology because the measurement is quick, repeatable, and nondestructive and because different lithologies often have strongly contrasting susceptibilities. The sensor used during Expedition 340 was a three-coil sensor providing deeper reading measurements, with a vertical resolution of ~40 cm. The MSS was run as a component of a Schlumberger tool string, using a specially developed data translation cartridge. For quality control and environmental correction, the MSS also measures internal tool temperature, z-axis acceleration, and low-resolution borehole conductivity.

Acoustic velocity

The Dipole Shear Sonic Imager (DSI) measures the transit times between sonic transmitters and an array of eight receivers. It combines replicate measurements, thus providing a measurement of compressional wave velocity (V_P) through sediment that is relatively free from the effects of formation damage and of an enlarged borehole (Schlumberger, 1989). Along with the monopole transmitters found on most sonic tools, it also has two cross-dipole transmitters, which allow an additional measurement of shear wave velocity (V_s). Dipole measurements are necessary to measure shear velocities in "slow" formations, where V_s is slower than the velocity in the borehole fluid. Such slow formations are typically encountered in deep ocean drilling.

Formation MicroScanner

The FMS provides high-resolution electrical resistivity images of borehole walls. The tool has four orthogonal arms and pads, each containing 16 button electrodes that are pressed against the borehole wall during the recording. The electrodes are arranged in

two diagonally offset rows of eight electrodes each. A focused current is emitted from the button electrodes into the formation, with a return electrode near the top of the tool. Resistivity of the formation at the button electrodes is derived from the intensity of current passing through the button electrodes. Processing transforms these measurements into oriented high-resolution images that reveal the geologic structures of the borehole wall. Features such as bedding, fracturing, slump folding, and bioturbation can be resolved; the images are oriented to magnetic north so that fabric analysis can be carried out and the dip and direction (azimuth) of planar features in the formation can be measured.

The maximum extension of the FMS caliper arms is 15 inches. In holes with a diameter >15 inches, pad contact will be inconsistent and FMS images may appear out of focus and too conductive. Irregular (rough) borehole walls will also adversely affect the images if contact with the wall is poor.

Accelerometry and magnetic field measurement

Three-component acceleration and magnetic field measurements were made with the General Purpose Inclinometry Tool (GPIT). The primary purpose of this tool, which incorporates a three-component accelerometer and a three-component magnetometer, is to determine the acceleration and orientation of the FMS-sonic tool string during logging. Thus, FMS images can be corrected for irregular tool motion, and the dip and direction (azimuth) of features in the FMS images can be determined.

Vertical seismic profile

In a vertical seismic profile (VSP) experiment, the VSI is anchored against the borehole wall at regularly spaced intervals and records acoustic waves generated by a seismic source positioned just below the sea surface. The main purpose of this experiment is to provide a direct measurement of the time necessary for seismic waves to travel from the surface to a given depth, to tie observations in the well, recorded as a function of depth, to reflections in seismic surveys, recorded as a function of time.

The VSI sensor is a three-axis geophone accelerometer built into a "shuttle" that is connected to the tool sonde. During Expedition 340, the VSI was anchored against the borehole wall at ~25 m depth intervals, depending on the quality of the borehole, and 5–15 recordings were taken at each station. The recorded waveforms were stacked, and a one-way traveltime was determined from the first breaks for each station. The seismic source used was a Sercel G. Gun parallel cluster, composed of two 250 in³ air guns separated by 1 m. It was positioned by one of the ship cranes ~30 m to the port side of the ship, at a total horizontal offset from the top of the well head of ~50 m, and maintained at a water depth of ~7 m.

In accordance with the requirements of the National Environmental Policy Act and the Endangered Species Act, all seismic activities were conducted during daytime and protected species observers kept watch for protected species for the duration of the zero-offset VSP. Any sight of protected species within the exclusion zone of 940 m (defined for water depths >1000 m) would interrupt the survey for 60 min after the last sighting or until the protected species were seen leaving the exclusion zone. Protected species observers began observations 1 h prior to the use of the seismic source, which started with a 30 min ramp-up procedure, gradually increasing the operational pressure and firing rate to provide time for undetected protected species to vacate the area. The same ramp-up procedure would be used when resuming activity after any interruption due to the sighting of protected species or whenever the gun was not fired for >30 min.

Auxiliary logging equipment

Cable head

The Schlumberger logging equipment head (LEH, or cable head) measures tension at the very top of the wireline tool string, which diagnoses difficulties in running the tool string up or down the borehole or when exiting or entering the drill string or casing.

Telemetry cartridges

Telemetry cartridges are used in each tool string to allow the transmission of data from the tools to the surface. The EDTC also includes a sodium iodide scintillation detector to measure the total natural gamma ray emission of the formation. This gamma ray log was used to match depths between the different passes and runs. In addition, the EDTC includes an accelerometer, the data from which can be used in real time to evaluate the efficiency of the WHC.

Joints and adapters

Because the tool strings combine tools of different generations and various designs, they include several adapters and joints between individual tools to allow communication, provide isolation, avoid interferences (mechanical and acoustic), terminate wirings, or position the tool properly in the borehole. Knuckle joints in particular were used to allow some of the tools such as the HRLA to remain centralized in the borehole while the overlying HLDS was pressed against the borehole wall.

All these additions are included and contribute to the total length of the tool strings in Figure **F11.**

Log data quality

The principal factor in log data quality is the condition of the borehole wall. If the borehole diameter varies over short intervals because of washouts or ledges, logs from tools that require good contact with the borehole wall (i.e., the density tool) may be degraded. Deep investigation measurements such as resistivity and sonic velocity, which do not require contact with the borehole wall, are generally less sensitive to borehole conditions. Very narrow ("bridged") sections will also cause irregular log results.

The quality of the logging depth determination depends on several factors. The depth of logging measurements is determined from the length of the cable played out from the winch on the ship. Uncertainties in logging depth occur because of ship heave, cable stretch, cable slip, or even tidal changes. Uncertainties in the depth of core samples occur because of incomplete core recovery or incomplete heave compensation. All of these factors generate some discrepency between core sample depths, logs, and individual logging passes. To minimize the effect of ship heave, a hydraulic WHC was used to adjust the wireline length for rig motion during wireline logging operations.

Wireline heave compensator

Evaluation of the WHC system continued during Expedition 340. The WHC system is designed to compensate for the vertical motion of the ship and maintain a steady motion of the logging tools. It uses vertical acceleration measurements made by a Motion Reference Unit (MRU), located under the rig floor near the center of gravity of the ship, to calculate the vertical motion of the ship. It then adjusts the length of the wireline by varying the distance between two sets of pulleys through which the cable passes. Real-time measurements of uphole (surface) and downhole acceleration are made simultaneously by the MRU and the EDTC, respectively. An LDEO-developed software package allows these data to be analyzed and compared in real time, displaying the actual motion of the logging tool string and enabling evaluation of the efficiency of the compensator.

Logging data flow and processing

Data for each wireline logging run were monitored in real time and recorded using the Schlumberger MAXIS 500 system. They were then copied to the shipboard processing stations for preliminary processing. Typically the main pass of the triple combo was used as a reference to which other passes were interactively depth matched. After depth matching, all logging depths were shifted to the seafloor based on a step in the gamma ray logs. These data were made available to the science party within a few days of their acquisition.

Downhole log data were also transferred onshore to LDEO for standardized data processing. The main part of the processing is depth matching to remove depth offsets between different logging passes, which results in a new depth scale: wireline log matched depth below seafloor (WMSF). Also, corrections are made to certain tools and logs (e.g., FMS images are corrected for tool acceleration), documentation for the logs (with an assessment of log quality) is prepared, and data are converted to ASCII for the conventional logs and to SEG-Y for the VSP data. Schlumberger GeoQuest's GeoFrame software package is used for most of the processing.

Core-log-seismic integration

A depth-traveltime relationship must be determined at each site to correlate core and log data acquired in depth with seismic reflection measurements that are a function of traveltime. A direct measurement of the depth-traveltime relationship is given by the first arrival times in the VSP (see **"Vertical seismic profile"**).

A depth-traveltime relationship can also be estimated by constructing synthetic seismograms, which are computed from reflection coefficients obtained from contrasts in the V_P and density logs, to match the seismic traces closest to the borehole. Synthetic seismograms were calculated using the IESX seismic interpretation package (part of the Schlumberger GeoFrame software suite), which allows for interactively adjusting the depth-traveltime relationship until a good match is achieved between features in the synthetic seismogram and in the recorded seismic data. A calibrated depth-traveltime relationship allows for the most accurate correlation of the borehole log and core data with seismic reflection features.

References

ASTM International, 1990. Standard method for laboratory determination of water (moisture) content of soil and rock (Standard D2216–90). In *Annual Book of ASTM Standards for Soil and Rock* (Vol. 04.08): Philadelphia (Am. Soc. Testing Mater.). [revision of D2216-63, D2216-80]

Barker, R.W., 1961. Taxonomic notes on the species figured by H.B. Brady in his report on the Foraminifera dredged by H.M.S. *Challenger* during the years 1873–1876. *Spec. Publ.—Soc. Econ. Paleontol. Minearl.,* 9:1–238.

Blum, P., 1997. Physical properties handbook: a guide to the shipboard measurement of physical properties of

deep-sea cores. *ODP Tech. Note,* 26. doi:10.2973/odp.tn.26.1997

Bouma, A.H., 1962. *Sedimentology of Some Flysch Deposits: A Graphic Approach to Facies Interpretation:* Amsterdam (Elsevier).

British Standards Institution, 1990. *Methods of Test for Soils for Civil Engineering Purposes* (Pt. 2): *Classification Tests* (Rep. BS 1377): London (British Standards Inst.).

Cande, S.C., and Kent, D.V., 1995. Revised calibration of the geomagnetic polarity timescale for the Late Cretaceous and Cenozoic. *J. Geophys. Res., [Solid Earth],* 100(B4):6093–6095. doi:10.1029/94JB03098

Clark, S.P. (Ed.), 1966. *Handbook of Physical Constants.* Mem.—Geol. Soc. Am., 97.

Ellis, B.F., and Messina, A., 1940. *Catalogue of Foraminifera.* Spec. Publ., Am. Mus. Nat. Hist.

Ellis, D.V., and Singer, J.M., 2007. *Well Logging for Earth Scientists* (2nd ed.): New York (Elsevier).

Evans, H.B., 1965. GRAPE—a device for continuous determination of material density and porosity. *Trans. SPWLA Annu. Logging Symp.:* 6(2):B1–B25.

Expedition 330 Scientists, 2012. Methods. *In* Koppers, A.A.P., Yamazaki, T., Geldmacher, J., and the Expedition 330 Scientists, *Proc. IODP,* 330: Tokyo (Integrated Ocean Drilling Program Management International, Inc.). doi:10.2204/iodp.proc.330.102.2012

Expedition 334 Scientists, 2012. Methods. *In* Vannucchi, P., Ujiie, K., Stroncik, N., Malinverno, A., and the Expedition 334 Scientists, *Proc. IODP,* 334: Tokyo (Integrated Ocean Drilling Program Management International, Inc.). doi:10.2204/iodp.proc.334.102.2012

Fuller, M., Molina-Garza, R., Touchard, Y., and Kidane, T., 2006. Paleomagnetic records from carbonate legs in the Southern Oceans and attendant drilling and coring related effects. *In* Sager, W.W., Acton, G.D., Clement, B.M., and Fuller, M. (Eds.), *ODP Contributions to Paleomagnetism.* Phys. Earth Planet. Int., 156(3–4):242–260. doi:10.1016/j.pepi.2005.08.007

Galluzzo, J.J., Sen Gupta, B.K., and Pujos, M., 1990. Holocene deep-sea foraminifera of the Grenada Basin. *J. Foraminiferal Res.,* 20(3):195–211. doi:10.2113/gsjfr.20.3.195

Gartner, S., 1977. Calcareous nannofossil biostratigraphy and revised zonation of the Pleistocene. *Mar. Micropaleontol.,* 2:1–25. doi:10.1016/0377-8398(77)90002-0

Gieskes, J.M., Gamo, T., and Brumsack, H., 1991. Chemical methods for interstitial water analysis aboard *JOIDES Resolution.* ODP Tech. Note, 15. doi:10.2973/odp.tn.15.1991

Goldberg, D., 1997. The role of downhole measurements in marine geology and geophysics. *Rev. Geophys.,* 35(3):315–342. doi:10.1029/97RG00221

Graber, K.K., Pollard, E., Jonasson, B., and Schulte, E. (Eds.), 2002. Overview of Ocean Drilling Program engineering tools and hardware. *ODP Tech. Note,* 31. doi:10.2973/odp.tn.31.2002

Hansbo, S., 1957. A new approach to the determination of the shear strength of clay by the fall-cone test. *R. Swed. Geotech. Inst., Proc.,* 14.

Harms, J.C., and Choquette, P.W., 1965. Geologic evaluation of a gamma-ray porosity device. *Trans. SPWLA Annu. Logging Symp.:* 6(2):C1–C37.

Hay, W.W., 1970. Calcareous nannofossils from cores recovered on Leg 4. *In* Bader, R.G., Gerard, R.D., et al., *Init. Repts. DSDP,* 4: Washington, DC (U.S. Govt. Printing Office), 455–501. doi:10.2973/dsdp.proc.4.123.1970

Hayward, B.W., and Kawagata, S., 2005. Extinct foraminifera figured in Brady's *Challenger* report. *J. Micropaleontol.,* 24(2):171–175. doi:10.1144/jm.24.2.171

Heesemann, M., Villinger, H., Fisher, A.T., Tréhu, A.M., and White, S., 2006. Data report: testing and deployment of the new APCT-3 tool to determine in situ temperatures while piston coring. *In* Riedel, M., Collett, T.S., Malone, M.J., and the Expedition 311 Scientists. *Proc. IODP,* 311: Washington, DC (Integrated Ocean Drilling Program Management International, Inc.). doi:10.2204/iodp.proc.311.108.2006

House, C.H., Cragg, B.A., Teske, A., and the Leg 201 Scientific Party, 2003. Drilling contamination tests during ODP Leg 201 using chemical and particulate tracers. *In* D'Hondt, S.L., Jørgensen, B.B., Miller, D.J., et al., *Proc. ODP, Init. Repts.,* 201: College Station, TX (Ocean Drilling Program), 1–19. doi:10.2973/odp.proc.ir.201.102.2003

Kameo, K., and Bralower, T.J., 2000. Neogene calcareous nannofossil biostratigraphy of Sites 998, 999, and 1000, Caribbean Sea. *In* Leckie, R.M., Sigurdsson, H., Acton, G.D., and Draper, G. (Eds.), *Proc. ODP, Sci. Results,* 165: College Station, TX (Ocean Drilling Program), 3–17. doi:10.2973/odp.proc.sr.165.012.2000

Keenan, J.H., Keyes, F.G., Hill, P.G., and Moore, J.G., 1978. *Steam Tables: Thermodynamic Properties of Water, Including Vapor, Liquid, and Solid Phases:* New York (John Wiley & Sons).

Kennett, J.P., and Srinivasan, M.S., 1983. *Neogene Planktonic Foraminifera: A Phylogenetic Atlas:* Stroudsburg, PA (Hutchinson Ross).

Kvenvolden, K.A., and McDonald, T.J., 1986. Organic geochemistry on the *JOIDES Resolution*—an assay. *ODP Tech. Note,* 6: College Station, TX (Ocean Drilling Program). doi:10.2973/odp.tn.6.1986

Le Bas, M.J., Le Maitre, R.W., and Woolley, A.R., 1992. The construction of the total alkali-silica chemical classification of volcanic rocks. *Mineral. Petrol.,* 46(1):1–22. doi:10.1007/BF01160698

Loeblich, A.R., and Tappan, H., 1988. *Foraminiferal Genera and Their Classification* (Vol. 2): New York (Van Nostrand Reinhold Co.).

Lovell, M.A., Harvey, P.K., Brewer, T.S., Williams, C., Jackson, P.D., and Williamson, G., 1998. Application of FMS images in the Ocean Drilling Program: an overview. *In* Cramp, A., MacLeod, C.J., Lee, S.V., and Jones, E.J.W. (Eds.), *Geological Evolution of Ocean Basins: Results from the Ocean Drilling Program.* Geol. Soc. Spec. Publ., 131(1):287–303. doi:10.1144/GSL.SP.1998.131.01.18

Manheim, F.T., 1966. A hydraulic squeezer for obtaining interstitial waters from consolidated and unconsolidated sediments. *Geol. Surv. Prof. Pap. (U.S.),* 550-C:256–261.

Munsell Color Company, Inc., 1994. *Munsell Soil Color Chart* (Revised ed.): Newburgh, MD (Munsell Color).

Okada, H., and Bukry, D., 1980. Supplementary modification and introduction of code numbers to the low-latitude coccolith biostratigraphic zonation (Bukry, 1973; 1975). *Mar. Micropaleontol.,* 5:321–325. doi:10.1016/0377-8398(80)90016-X

Poag, C.W., 1981. *Ecologic Atlas of Benthic Foraminifera of the Gulf of Mexico:* Stroudsburg, PA (Hutchinson Ross).

Ratcliffe, E.H., 1960. The thermal conductivities of ocean sediments. *J. Geophys. Res.,* 65(5):1535–1541. doi:10.1029/JZ065i005p01535

Richter, C., Acton, G., Endris, C., and Radsted, M., 2007. Handbook for shipboard paleomagnetists. *ODP Tech. Note,* 34. doi:10.2973/odp.tn.34.2007

Rider, M.H., 1996. *The Geological Interpretation of Well Logs* (2nd ed.): Caithness (Whittles Publ.).

Schlumberger, 1989. *Log Interpretation Principles/Applications:* Houston (Schlumberger Educ. Serv.), SMP–7017.

Serra, O., 1984. *Fundamentals of Well-Log Interpretation* (Vol. 1): *The Acquisition of Logging Data:* Amsterdam (Elsevier).

Serra, O., 1986. *Fundamentals of Well-Log Interpretation* (Vol. 2): *The Interpretation of Logging Data.* Amsterdam (Elsevier).

Serra, O., 1989. *Formation MicroScanner Image Interpretation:* Houston (Schlumberger Educ. Serv.), SMP-7028.

Talling, P.J., Amy, L.A., Wynn, R.B., Peakall, J., and Robinson, M., 2004. Beds comprising debrite sandwiched within co-genetic turbidite: origin and widespread occurrence in distal depositional environments. *Sedimentology,* 51(1):163–174. doi:10.1111/j.1365-3091.2004.00617.x

Taylor, B., Huchon, P., Klaus, A., et al., 2000. *Proc. ODP, Init. Repts.,* 180: College Station, TX (Ocean Drilling Program). doi:10.2973/odp.proc.ir.180.2000

van Morkhoven, F.P.C.M., Berggren, W.A., and Edwards, A.S., 1986. *Cenozoic Cosmopolitan Deep-Water Benthic Foraminifera.* Bull. Cent. Rech. Explor.—Prod. Elf-Aquitaine, 11.

Vasiliev, M.A., Blum, P., Chubarian, G., Olsen, R., Bennight, C., Cobine, T., Fackler, D., Hastedt, M., Houpt, D., Mateo, Z., and Vasilieva, Y.B., 2011. A new natural gamma radiation measurement system for marine sediment and rock analysis. *J. Appl. Geophys.,* 75:455–463. doi:10.1016/j.jappgeo.2011.08.008

Wade, B.S., Pearson, P.N., Berggren, W.A., and Pälike, H., 2011. Review and revision of Cenozoic tropical planktonic foraminiferal biostratigraphy and calibration to the geomagnetic polarity and astronomical time scale. *Earth-Sci. Rev.,* 104(1–3):111–142. doi:10.1016/j.earscirev.2010.09.003

Watt, S.F.L., Talling, P.J., Vardy, M.E., Heller, V., Hühnerbach, V., Urlaub, M., Sarkar, S., Masson, D.G., Henstock, T.J., Minshull, T.A., Paulatto, M., Le Friant, A., Lebas, E., Berndt, C., Crutchley, G.J., Karstens, J., Stinton, A.J., and Maeno, F., 2012. Combinations of volcanic-flank and seafloor-sediment failure offshore Montserrat, and their implications for tsunami generation. *Earth Planet. Sci. Lett.,* 319–320:228–240. doi:10.1016/j.epsl.2011.11.032

Wentworth, C.K., 1922. A scale of grade and class terms for clastic sediments. *J. Geol.,* 30(5):377–392. doi:10.1086/622910

Wood, D.M., 1985. Some fall-cone tests. *Géotechnique,* 35(1):64–68. doi:10.1680/geot.1985.35.1.64

Zoth, G., and Haenel, R., 1988. Appendix: 1. *In* Haenel, R., Rybach, L., and Stegena, L. (Eds.), *Handbook of Terrestrial Heat-Flow Density Determination: with Guidelines and Recommendations of the International Heat Flow Commission:* Dordrecht (Kluwer Acad. Publ.), 449–4668.

Figure F1. Integrated Ocean Drilling Program (IODP) labeling scheme used for holes, cores, and sections, Expedition 340.
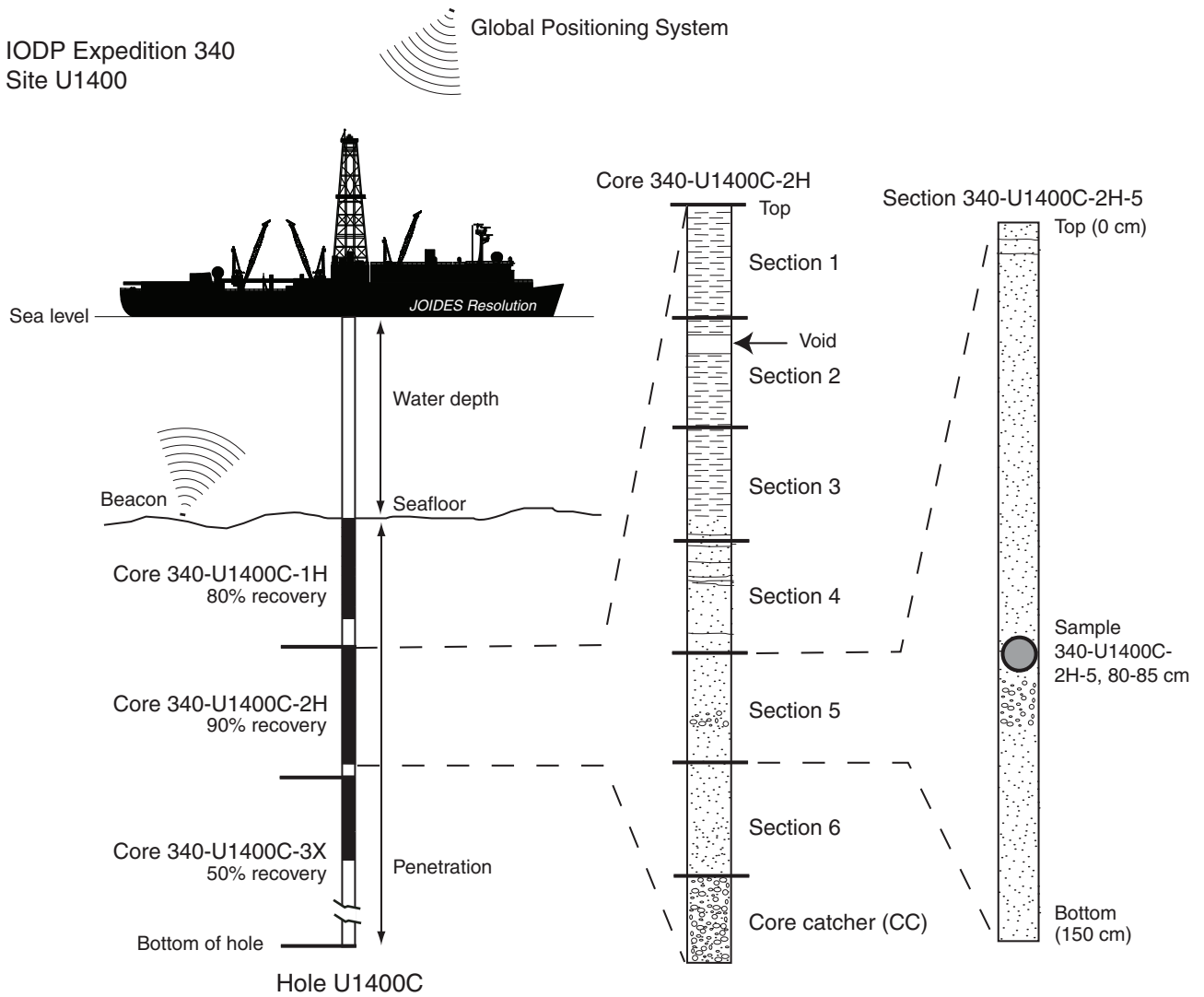
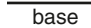**Figure F2.** Key to symbols used on graphical core logs, Expedition 340.

Grading patterns

Normally graded

or   Ungraded

Inversely graded

Sedimentary structures

Planar lamination

Cross lamination

Sharp base or top to layer
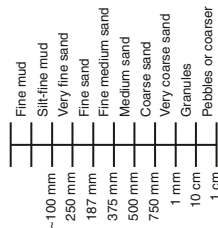
Erosional boundary

g   Green laminae (in hemipelagite)

Other symbols

√   Observation confirmed (sure)

?   Observation unsure/equivocal

base   Base of core barrel

Samples (voids in core)

PAL   Paleontology

IW   Interstitial water

WR   Whole round

Grain size

Fine mud | Silt-fine mud | Very fine sand | Fine sand | Fine medium sand | Medium sand | Coarse sand | Very coarse sand | Granules | Pebbles or coarser

~100 mm | 250 mm | 187 mm | 375 mm | 500 mm | 750 mm | 1 mm | 10 cm | 1 cm
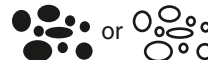
Abbreviations

turb.   Turbidite

v.   Very

Bioturbation intensity

Bioturbation

Strong bioturbation

Burrow infilled

Lithologies

or   Clasts (see comments for composition)

Isolated clast

Coarse sand

Dark gray or black ash

HP or hp   Hemipelagic mud

ⓐ   Probable fallout layer

Visual composition of turbidites

Ⓑ   Bioclastic-dominated turbidite

Ⓜ   Mixed bioclastic-volcanic turbidite

Ⓥ   Volcaniclastic-dominated turbidite

Drilling disturbance

Strong disturbance

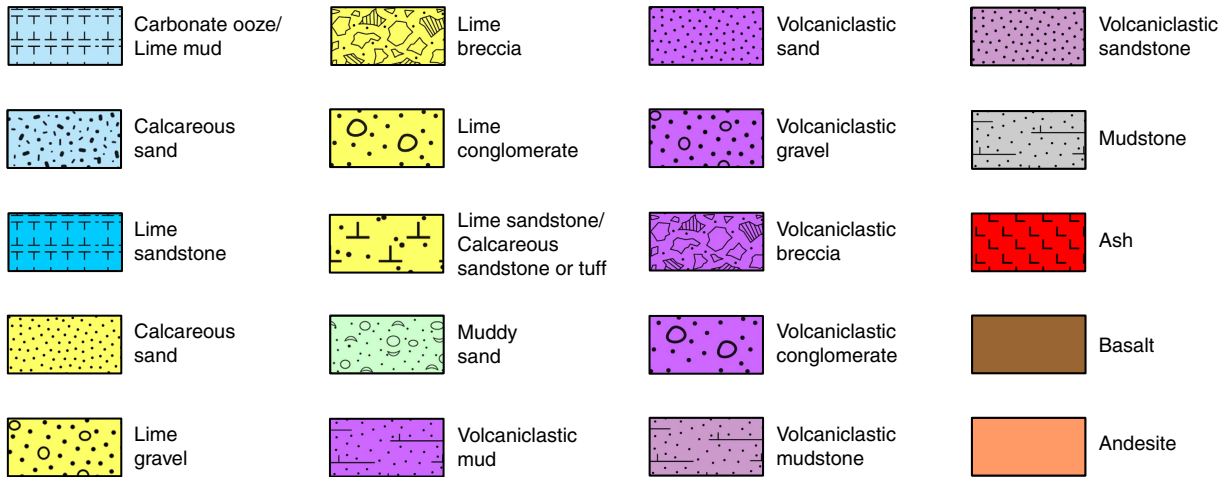Weak disturbance

No disturbance

Drilling biscuit

Matrix composition from optical microscope

15% mass lava, 5% vesic lava, 25% carbonate, 8% pumice, etc.
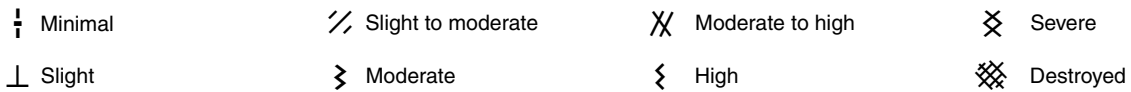
Arrow shows sample location

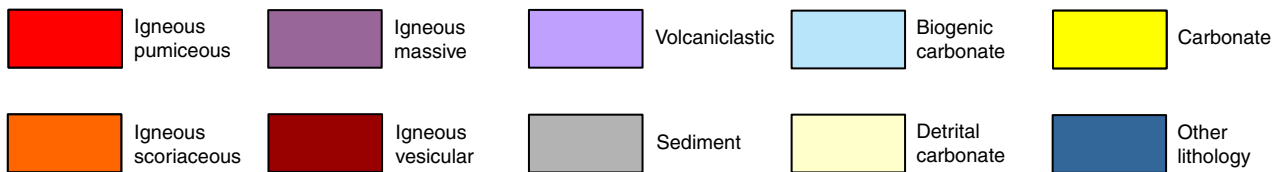**Figure F3.** Key to lithologies and symbols used in DESClogik, Expedition 340.
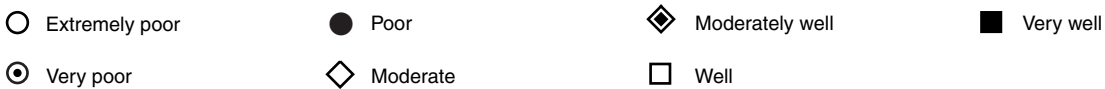
Lithology

Carbonate ooze/ Lime mud	Lime breccia	Volcaniclastic sand	Volcaniclastic sandstone
Calcareous sand	Lime conglomerate	Volcaniclastic gravel	Mudstone
Lime sandstone	Lime sandstone/ Calcareous sandstone or tuff	Volcaniclastic breccia	Ash
Calcareous sand	Muddy sand	Volcaniclastic conglomerate	Basalt
Lime gravel	Volcaniclastic mud	Volcaniclastic mudstone	Andesite

Drilling disturbance

Minimal	Slight to moderate	Moderate to high	Severe
Slight	Moderate	High	Destroyed

Matrix and clast type

Igneous pumiceous	Igneous massive	Volcaniclastic	Biogenic carbonate	Carbonate
Igneous scoriaceous	Igneous vesicular	Sediment	Detrital carbonate	Other lithology

Matrix sorting

Extremely poor	Poor	Moderately well	Very well
Very poor	Moderate	Well	

Grading type

Normal	Reverse

Shipboard samples

TS	Thin section	**PMG**	Paleomagnetism	**CRB**	Carbonate	**PP**	Physical properties
HS	Headspace gas	**SED**	Sediment	**MBIO**	Microbiology	**XRD**	X-ray diffraction
PAL	Paleontology	**NAN**	Nannofossils	**FOR**	Foraminifers - planktonic/benthic	**MADC**	Moisture and density method C
IW	Interstitial water	**ICP**	ICP-AES analysis				

Figure F4. Example of visual core description (VCD), Expedition 340.

Hole 340-U1397A-11H Section 3, Top of Section: 76.51 CSF-A (m)

Complex mixture of stacked graded sand-mud units, and hemipelagic mud. Upper part is base of debris flow deposit.
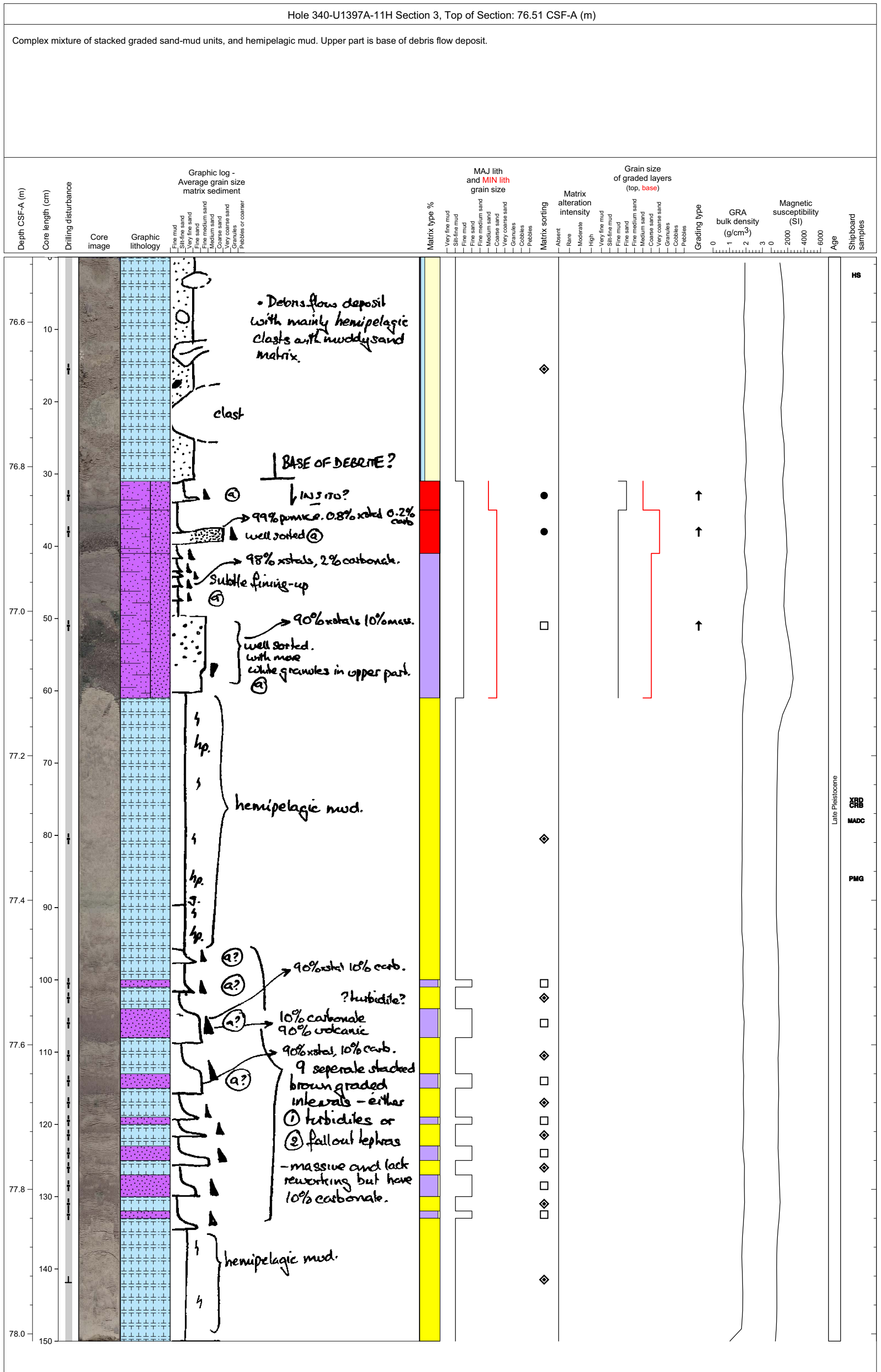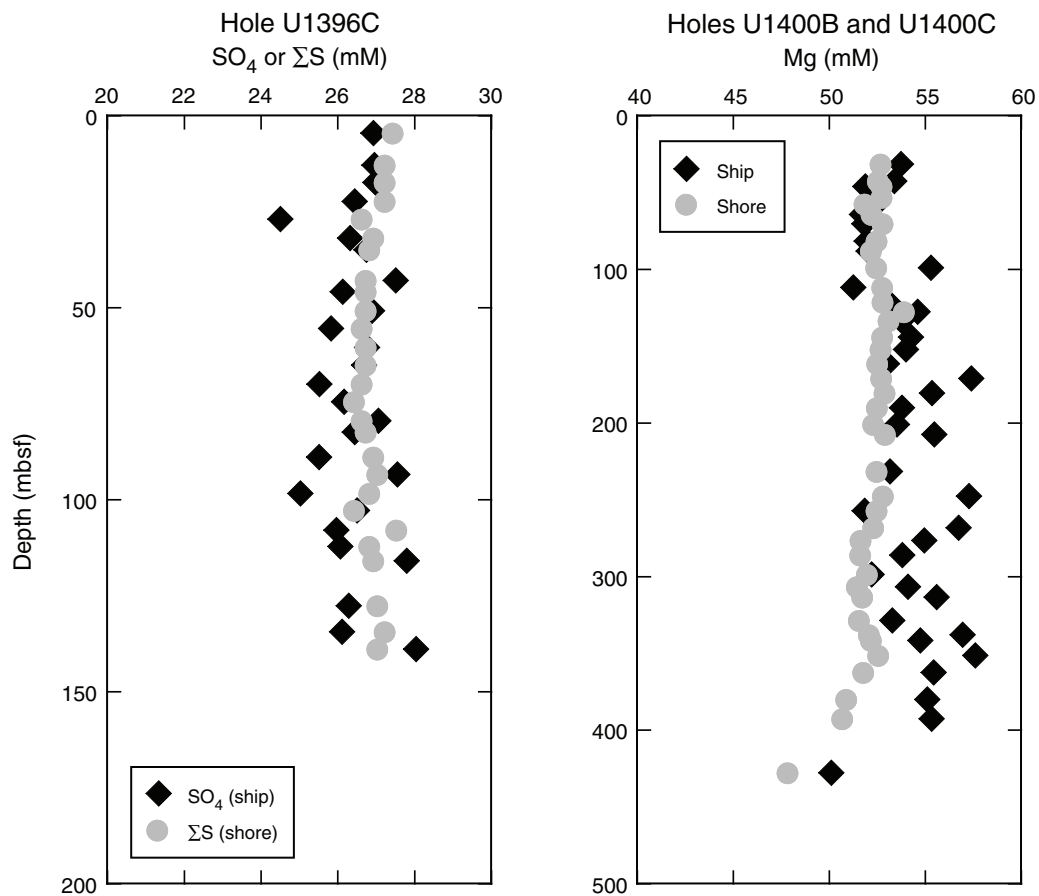
Figure F5. Examples of pore fluid data run at sea (ship) and back on shore (shore), Expedition 340.

Figure F6. Type I: carbonates. Type I includes calcite (Cc), Mg-rich calcite (Mg-Cc), and aragonite (Arag), along with minor volcanic minerals: mainly plagioclase (Plag) and highly variable clay minerals contents (smectite [Sm] and kaolinite [Kaol]; see Fig. F8). Samples 340-U1394B-11H-6, 17–18 cm (green); 15H-2, 96–98 cm (black); 16H-4, 50–51 cm (blue); and 17H-CC, 23–24 cm (red).
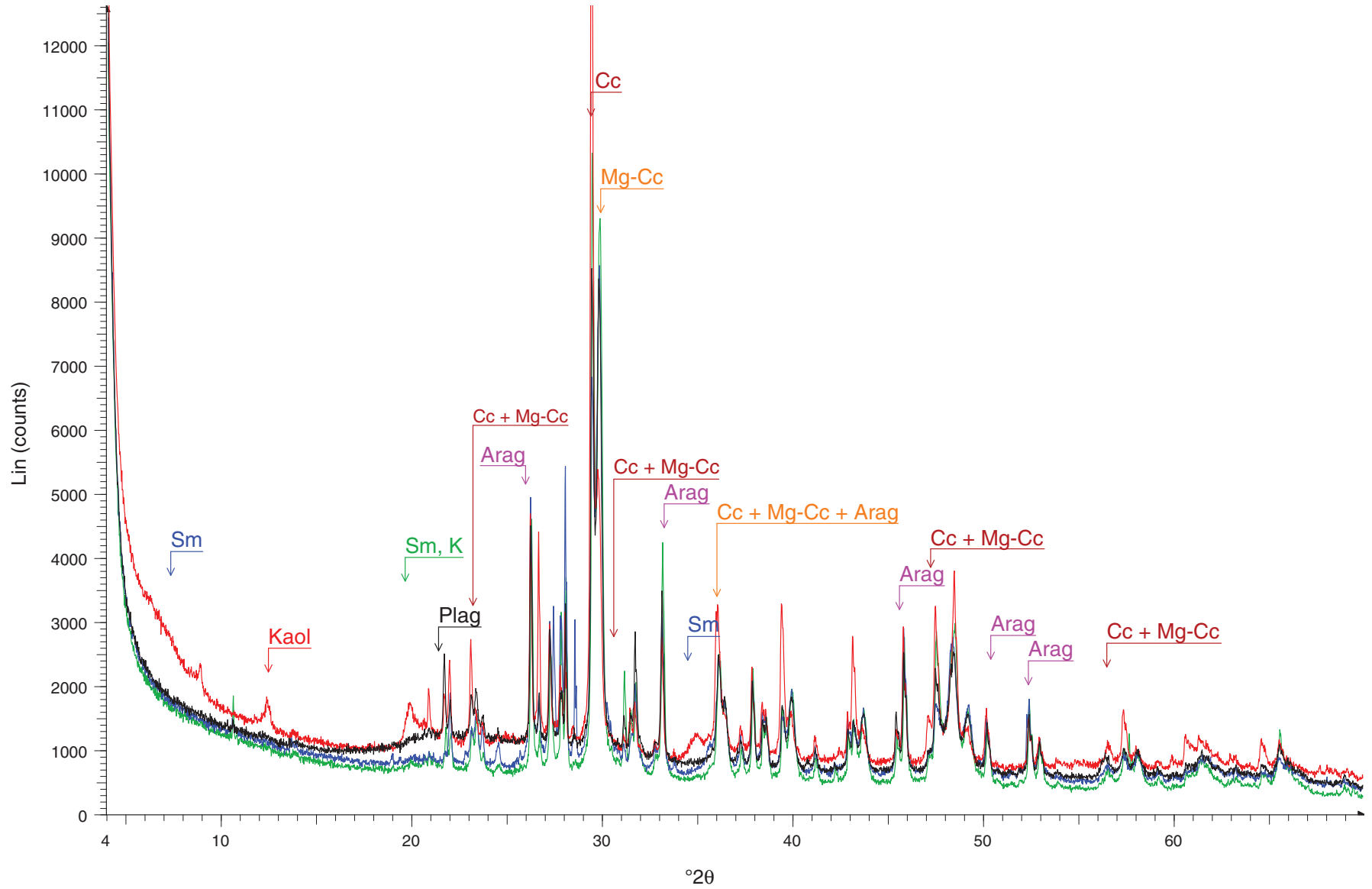
Figure F7. Type II: volcanics. Type II includes silicates (plagioclase, pyroxenes [difficult to identify; characteristic lines masked by plagioclase lines], and hornblende [Hb]), glass (bulge under the main plagioclase lines), minor and variable carbonates (mainly calcite), and highly variable clay mineral contents (smectite and kaolinite; see Fig. F8). An = anorthite. Samples 340-U1394B-12H-3, 129–130 cm (black), and 3H-1, 72–74 cm (red).
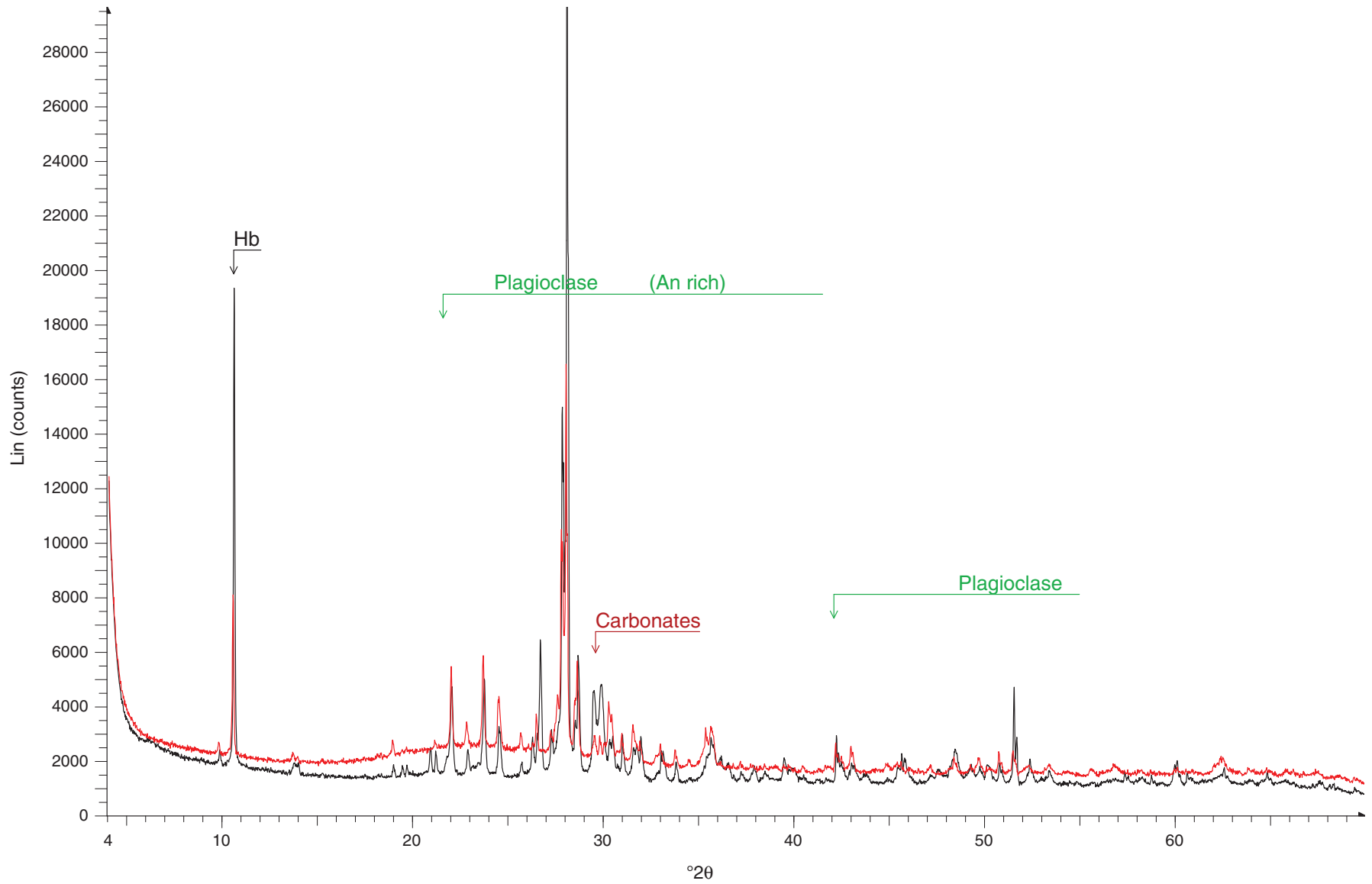
Figure F8. Type IV: clay minerals. Type IV includes smectites (Sm; continuous series of lines in the 5°–9°2θ range), kaolinite, and glauconite. Samples 340-U1395A-18X-1, 39–40 cm (black); 22X-1, 39–40 cm (red); and 18X-3, 58–60 cm (blue).
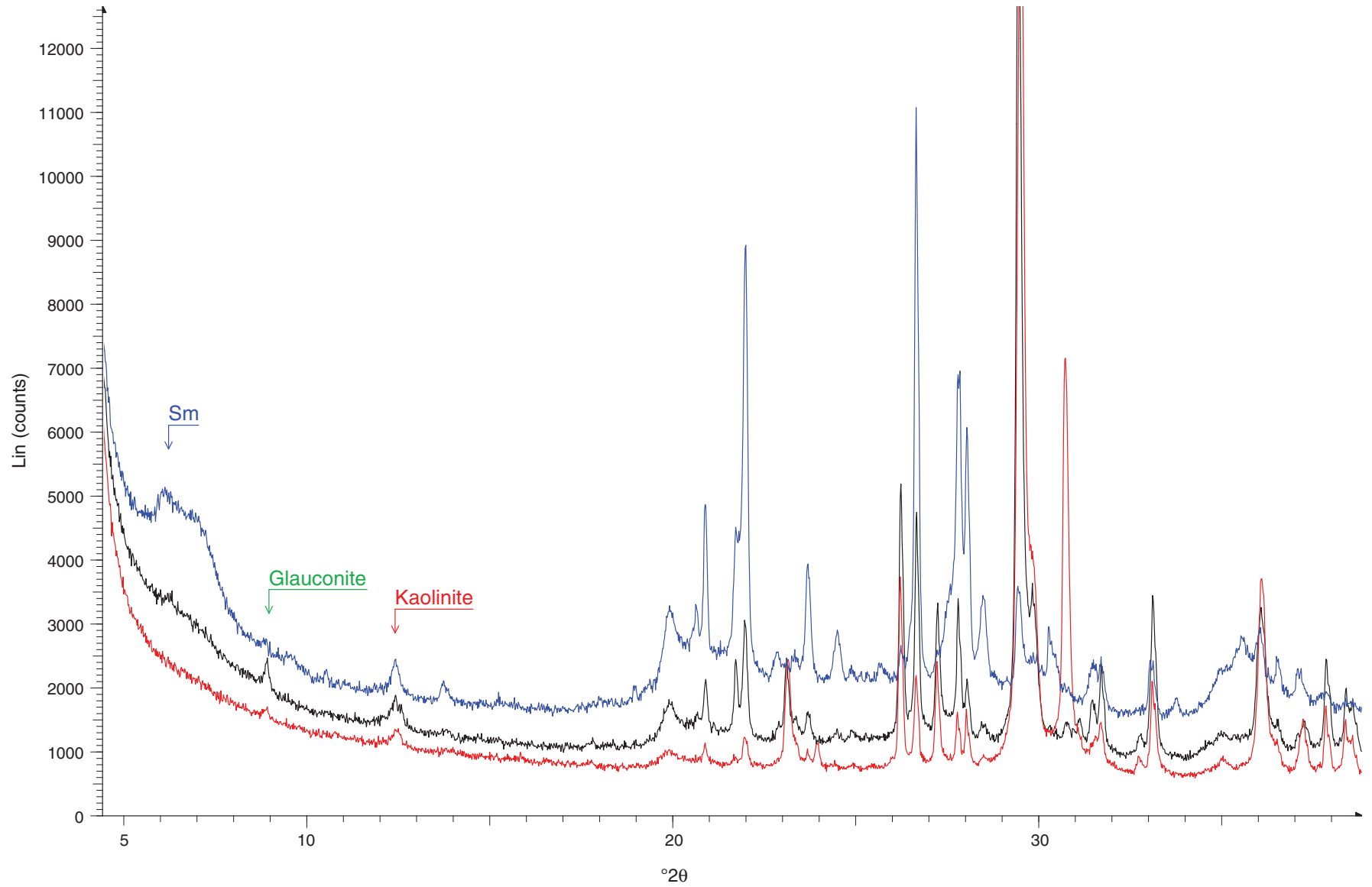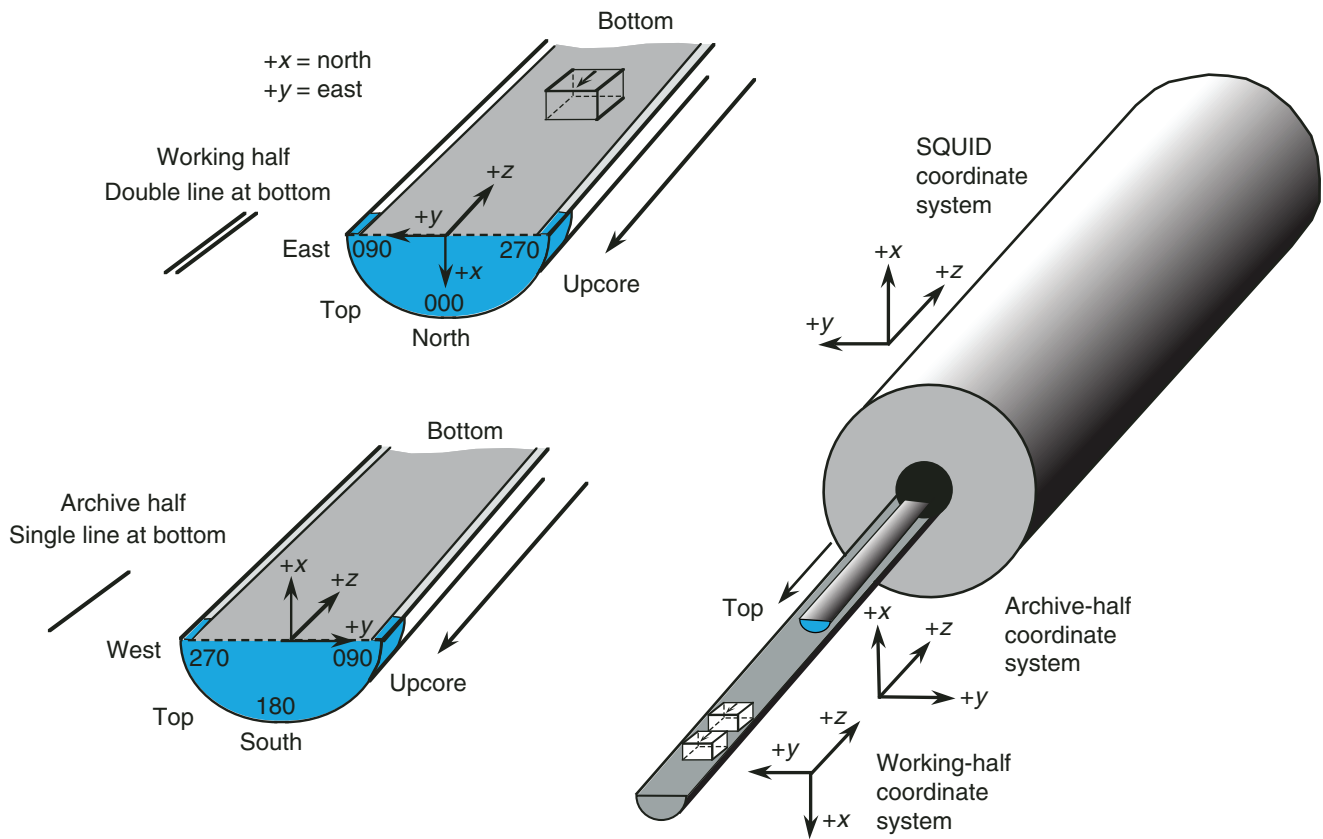
Figure F9. Variations in relative abundances of carbonates. Cc = calcite, Mg-Cc = Mg-rich calcite, Arag = aragonite. Samples 340-U1395A-11H-2, 103–104 cm; 1H-2, 55–56 cm; and 1H-1, 85–86 cm.
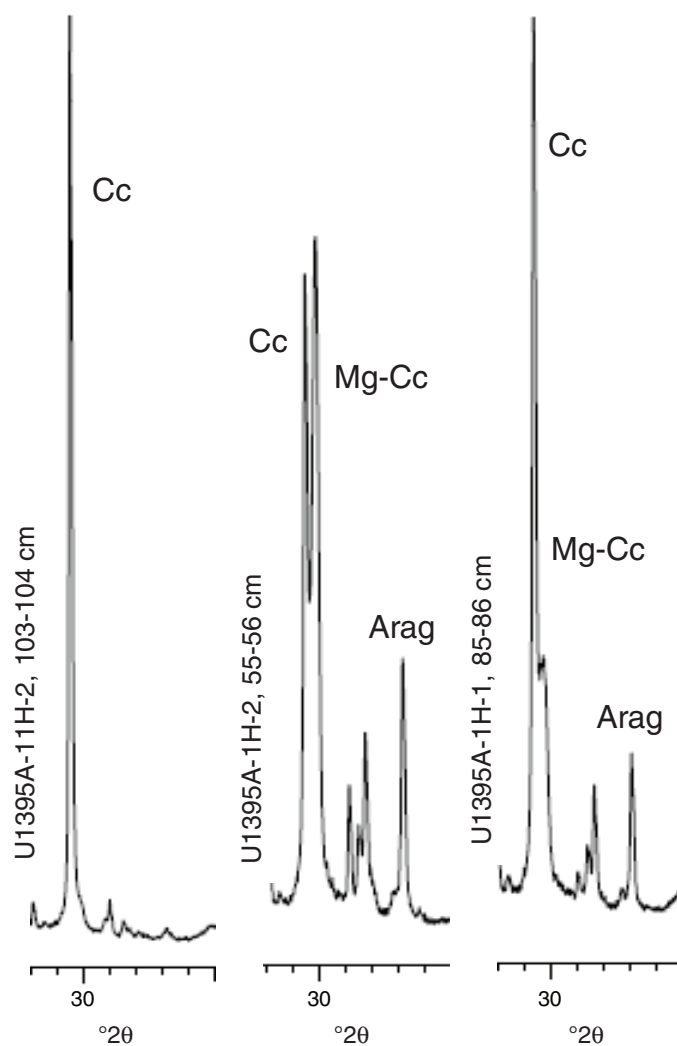
Figure F10. IODP core orientation system (from Richter et al., 2007). SQUID = superconducting quantum interference device.

Figure F11. Wireline tool strings used during Expedition 340. LEH-QT = Logging Equipment Head–Q tension, EDTC = Enhanced Digital Telemetry Cartridge, HLDS = Hostile Environment Litho-Density Sonde, HRLA = High-Resolution Laterolog Array, HNGS = Hostile Environment Natural Gamma Ray Sonde, MSS = Magnetic Susceptibility Sonde, FMS = Formation MicroScanner, DSI = Dipole Shear Sonic Imager, GPIT = General Purpose Inclinometry Tool, VSI = Versatile Seismic Imager.
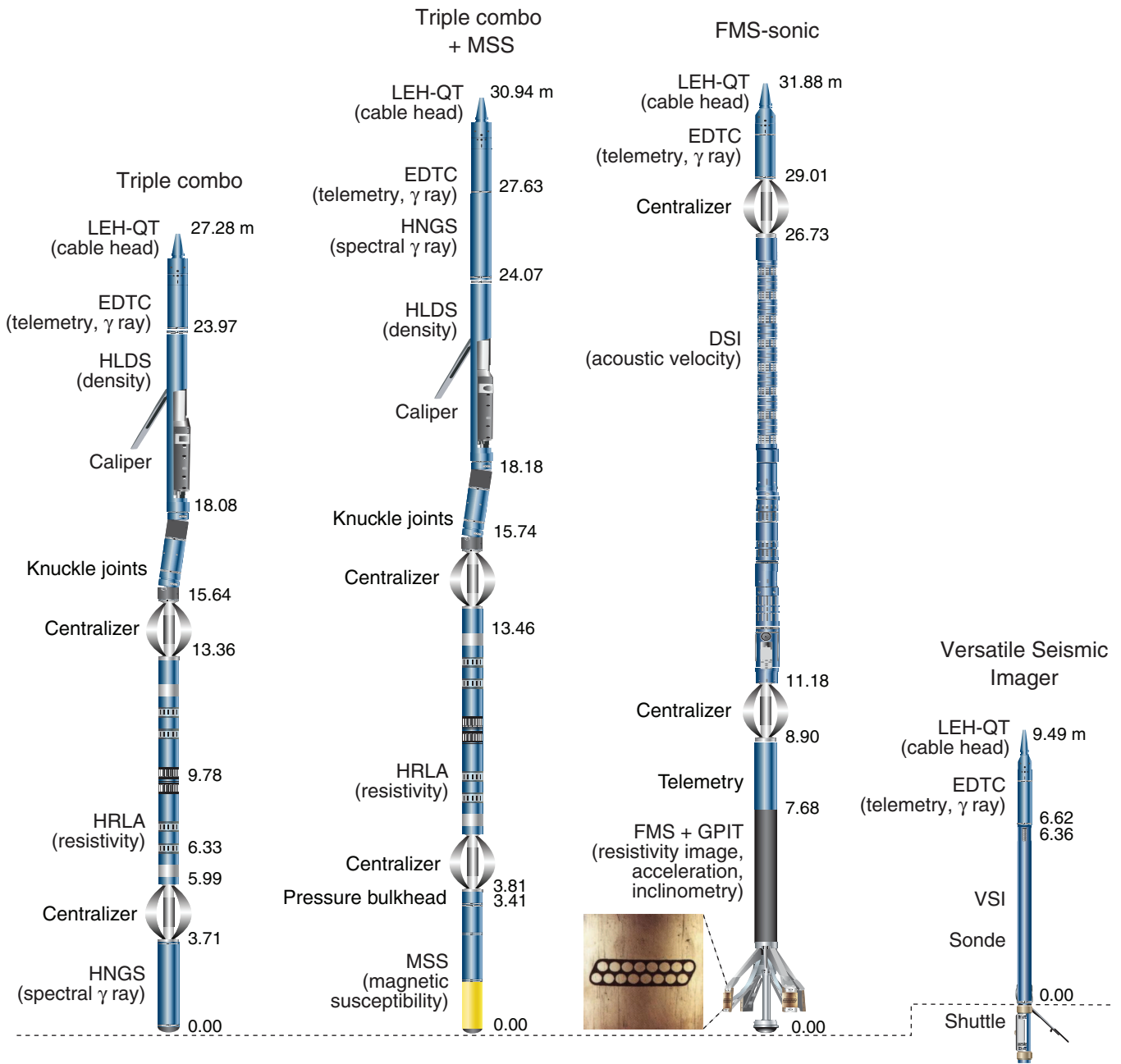
Table T1. Calcareous nannofossil datum events used for age estimates, Expedition 340.

Nannofossil datum	Calibrated age (Ma)	Source
B acme *Emiliania huxleyi*	0.085	Kameo and Bralower, 2000
B *Emiliania huxleyi*	0.250	Kameo and Bralower, 2000
T *Pseudoemiliania lacunosa*	0.410	Kameo and Bralower, 2000
B *Gephyrocapsa parallela*	0.950	Kameo and Bralower, 2000
B *Gephyrocapsa oceanica*	1.650	Kameo and Bralower, 2000
B *Gephyrocapsa caribbeanica*	1.730	Kameo and Bralower, 2000
T *Discoaster brouweri*	1.970	Kameo and Bralower, 2000
T *Discoaster pentaradiatus*	2.380	Kameo and Bralower, 2000
T *Discoaster surculus*	2.540	Kameo and Bralower, 2000
T *Discoaster tamalis*	2.740	Kameo and Bralower, 2000
T *Reticulofenestra pseudoumbilicus*	3.800	Kameo and Bralower, 2000
T *Amaurolithus primus*	4.370	Kameo and Bralower, 2000

Table T2. Planktonic foraminifer datum events used for age estimates, Expedition 340.

Planktonic foraminifer datum	Calibrated age (Ma)	Source
T *Globorotalia flexuosa*	0.07	Wade et al., 2011
B *Globigerinella calida*	0.22	Wade et al., 2011
B *Globorotalia flexuosa*	0.40	Wade et al., 2011
T *Globorotalia tosaensis*	0.61	Wade et al., 2011
T *Globigerinoides fistulosus*	1.88	Wade et al., 2011
B *Globorotalia truncatulinoides*	1.93	Wade et al., 2011
T *Globigerinoides extremus*	1.98	Wade et al., 2011
T *Globorotalia exillis*	2.10	Wade et al., 2011
T *Globorotalia pertenuis*	2.30	Wade et al., 2011
T *Globorotalia miocenia*	2.39	Wade et al., 2011
T *Globorotalia multicamerata*	2.99	Wade et al., 2011
T *Dentoglobigerina altispira*	3.47	Wade et al., 2011
T *Sphaeroidinellopsis seminulina*	3.59	Wade et al., 2011
T *Pulleniatina primalis*	3.65	Wade et al., 2011
T *Globorotalia margaritae*	3.84	Wade et al., 2011
T *Globoturborotalita nepenthes*	4.37	Wade et al., 2011

Table T3. Geomagnetic polarity timescale (GPTS; Cande and Kent, 1995).

Normal polarity interval (Ma)	Polarity chron name
0.000–0.780	C1n
0.990–1.070	C1r.1n
1.770–1.950	C2n
2.140–2.150	C2r.1n
2.581–3.040	C2An.1n
3.110–3.220	C2An.2n
3.330–3.580	C2An.3n
4.180–4.290	C3n.1n
4.480–4.620	C3n.2n

Table T4. Downhole measurements made by wireline tool strings, Expedition 340.

Tool string	Tool	Measurement	Sampling interval (cm)	Vertical resolution (cm)
Triple combo	EDTC	Total gamma ray	5 and 15	30
Triple combo + MSS	HNGS	Spectral gamma ray	15	20–30
	HLDS	Bulk density	2.5 and 15	38
	HRLA	Resistivity	15	30
	MSS	Magnetic susceptibility	2.54	40
FMS-sonic	EDTC	Total gamma ray	5 and 15	30
	DSI	Acoustic velocity	15	107
	GPIT	Tool orientation and acceleration	4	15
	FMS	Microresistivity	0.25	1
Versatile Seismic Imager	VSI	One-way acoustic traveltime	Stations at 10–25 m	NA
	EDTC	Total gamma ray	5 and 15	30

All tool and tool string names except the MSS are trademarks of Schlumberger. Sampling intervals are based on optimal logging speed. Acoustic imaging approximate vertical resolution is 500 kHz. NA = not applicable. For definitions of tool acronyms, see Table **T5.**

Table T5. Acronyms and units used for downhole wireline tools and measurements, Expedition 340.

Tool	Output	Description	Unit
EDTC		Enhanced Digital Telemetry Cartridge	
	GR	Total gamma ray	gAPI
	ECGR	Environmentally corrected gamma ray	gAPI
	EHGR	High-resolution environmentally corrected gamma ray	gAPI
HNGS		Hostile Environment Gamma Ray Sonde	
	HSGR	Standard (total) gamma ray	gAPI
	HCGR	Computed gamma ray (HSGR minus uranium contribution)	gAPI
	HFK	Potassium	wt%
	HTHO	Thorium	ppm
	HURA	Uranium	ppm
HLDS		Hostile Environment Litho-Density Sonde	
	RHOM	Bulk density	g/cm^3
	PEFL	Photoelectric effect	$barn/e^-$
	LCAL	Caliper (measure of borehole diameter)	Inch
	DRH	Bulk density correction	g/cm^3
HRLA		High-Resolution Laterolog Array Tool	
	RLAXXX	Apparent resistivity from computed focusing mode XXX	Ωm
	RT	True resistivity	Ωm
	MRES	Borehole fluid resistivity	Ωm
MSS		Magnetic Susceptibility Sonde	
	LSUS	Magnetic susceptibility, deep reading	Uncalibrated units
FMS		Formation MicroScanner	
	C1, C2	Orthogonal hole diameters	Inch
	P1AZ	Pad 1 azimuth	Degrees
		Spatially oriented resistivity images of borehole wall	
GPIT		General Purpose Inclinometry Tool	
	DEVI	Hole deviation	Degrees
	HAZI	Hole azimuth	Degrees
	Fx, Fy, Fz	Earth's magnetic field (three orthogonal components)	Degrees
	Ax, Ay, Az	Acceleration (three orthogonal components)	m/s^2
DSI		Dipole Shear Sonic Imager	
	DTCO	Compressional wave slowness	μs/ft
	DTSM	Shear wave slowness	μs/ft
	DT1	Shear wave slowness, lower dipole	μs/ft
	DT2	Shear wave slowness, upper dipole	μs/ft
VSI		Versatile Seismic Imager	
	1WTT	Acoustic traveltime	s